POLYMER STABILIZED NANOSUPENSIONS VIA FLASH NANOPRECIPITATION: PARTICLE FORMULATION, STRUCTURE AND FREEZE DRYING

A DISSERTATION SUBMITTED TO THE FACULTY OF THE GRADUATE SCHOOL OF THE UNIVERSITY OF MINNESOTA BY

KEVIN PUSTULKA

IN PARTIAL FULFILLMENT OF THE REQUIREMENTS
FOR THE DEGREE OF
MASTERS OF SCIENCE

ADVISOR: CHRISTOPHER MACOSKO

July 2012

Table of Contents

List of Figures

Chapter 1: An introduction to flash nanoprecipitation

Approximately 30-40% of new drug candidates have poor aqueous solubility, which leads to a low effective concentration in biofluids and therefore poor bioavailability. In fact, solubility is one of the most significant challenges when it comes to designing drug delivery systems [1]. Many of these hydrophobic drugs must be administered in formulation in order to overcome their hydrophobicity. One such example is paclitaxel.

Paclitaxel is one of today's leading cancer therapeutics, and although is shows high activity against cancer cell lines and tumors, it exhibits major challenges when it comes to effective delivery to tumors in vivo. One commercially available formulation of paclitaxel is Taxol®. Taxol® uses Cremophor EL®, a 50:50 mixture of polyethoxylated castor oil and ethanol, as the delivery agent [2]. While Cremophor EL® had previously been used to encapsulate insoluble drugs in micelles, the higher hydrophobicity of paclitaxel required five times as much Cremophor EL® for administration [3]. Due to the large amount of excipient required, Taxol® contains only 1 wt% paclitaxel. Cremophor EL® is also pharmacologically and biologically active, causing Taxol® to exhibit a variety of adverse side effects, most notably hypersensitivity [4]. Hypersensitivity refers to undesirable reactions produced by the normal immune system. In Taxol®, reactions occurred at a variety of doses and were characterized most frequently by dyspnea (shortness of breath), hypotension, bronchospasm, urticaria (hives), and erythematous rashes. Despite these side effects, the medical potential of paclitaxel was so great that Taxol® eventually won approval by the FDA [2]. However, it

is clear that a new drug delivery system that eliminated Cremophor EL® could greatly reduce the detrimental side effects.

A second formulation under the trademark Abraxane®, manufactured by Abraxis BioScience, is also available for the delivery of Paclitaxel. In Abraxane®, paclitaxel is complexed with albumin to form 130 nm stable nanoparticles in a solvent free formulation, which avoids all Cremophor EL® related toxicities. In addition, Abraxane® has a notably higher loading of paclitaxel (10 wt%) [5]. However, it presented no difference in overall survival as compared to Taxol® and also had a higher incidence of peripheral neuropathy, nausea, vomiting, and asthenia [6]. In the cases of both Taxol® and Abraxane®, the toxicity of paclitaxel on normal tissues is serious due to non-specific delivery, demonstrating the importance of selective delivery of paclitaxel to the tumor.

Nano-scale drug delivery systems show great promise for the delivery of insoluble drugs and can be devised to tune release kinetics, regulate biodistribution and minimize toxic side effects [7]. The nanometer size range enhances the ability of the drug delivery carriers by reducing the risk of undesired clearance from the body through the liver or spleen and minimizes uptake by the reticuloendothelial system [8]. Nano-scale drug delivery system are particulary important in cancer research due to their ability to exploit the anatomical and pathophysiological abnormalities of tumor tissue, particularly the vasculature via the enhanced permeation and retention (EPR) effect [9]. Rapidly growing tumor cells have a high requirement for nutrients. As a result, the tumors initiate and promote growth of new vascularization to meet that need [10]. The new blood vessels are irregular in shape, dilated, leaky or defective and the endothelial cells are poorly aligned or disorganized with large fenestrations [11, 12]. These leaky

vessels can therefore allow particles smaller than 200 nm, such as drug loaded nanoparticles, to pass through the vessel walls as shown in figure 1.1. The tumors also have poor lymphatic drainage. This means that the tumors drain slowly so the particles will be likely to stay inside the tumors [13, 14]. Particle size is therefore important when developing nano-scale drug delivery vehicles.

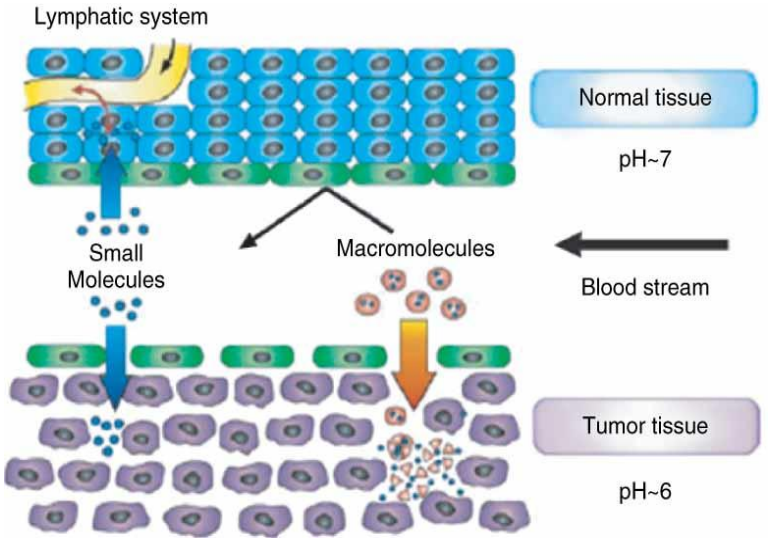

Figure 1.1: Anatomical differences between tumor tissue and normal tissue. The tumor tissue has leaky vessels, allowing small particles to pass through the vessel walls [15].

Several drug carrier systems have been developed such a liposomes [16], polymer vesicles [17], and micelles [18, 19] consisting of particles between 50 and 400 nm for the formulation of highly insoluble cancer therapeutics. However, the drug loading capacities of these systems are typically low (less than 20%) [20–22]. Higher drug loading formulations are desirable in nano sized carrier systems in order to let the drug localize with a higher dosage. One way to produce such carriers is to make kinetically stabilized nanoparticles via a process called flash nanoprecipitation.

Flash nanoprecipitation (FNP), developed by Prud'homme and coworkers [23, 24], is a promising technology for the encapsulation of hydrophobic drugs in a polymer based delivery vehicle. FNP involves the rapid impingement mixing of two miscible liquids in a confined space. Impinging jets consist of two high velocity linear jets of fluid

that collide to rapidly reduce the scale of segregation between the two fluid streams [23]. One of these jets consists of an organic solvent in which an amphiphilic diblock copolymer and a solute, such as a hydrophobic drug, are dissolved, while the other jet is a miscible antisolvent, such as water. When the two streams are mixed, particles are formed through the process of solvent shifting [25, 26]. The solvent shifts away from the solutes to its miscible antisolvent, while the antisolvent shifts in. This results in the supersaturation of the solutes, defined as the ratio of solubility of the solute in the organic phase to that in the mixed water and organic phase, and subsequent precipitation. The hydrophobic block and solute aggregate and are encapsulated in the core of the nanoparticle. The hydrophilic block forms a corona, or outer covering, that effectively stabilizes the particle by preventing aggregation of the nanoparticles and also solubilizes the particle in an aqueous environment. The advantages of FNP include a high drug encapsulation efficiency, high drug loading, and a well controlled particle size and size distribution [27, 28]. These properties are particularly appealing for cancer drugs due to the EPR effect.

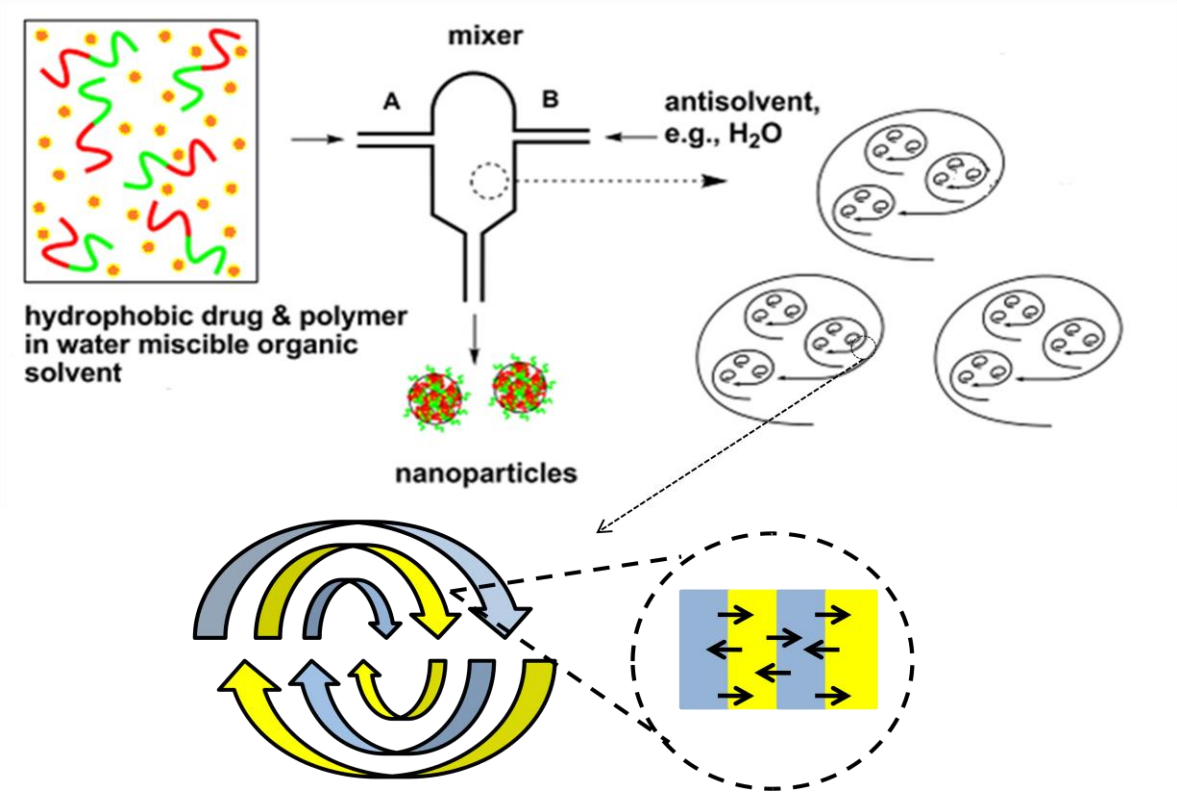

Figure 1.2: Schematic Diagram of the Flash Nanoprecipitation Process

Impinging jets were chosen due to their ability to deliver mixing times less than the characteristic time of the process. In order to achieve rapid mixing, a region of high turbulent energy dissipation must be produced and the process streams being mixed pass through the high intensity region. In impinging jets, a high energy dissipation occurs because the kinetic energy of each jet stream is converted into a turbulent-like motion through collision and redirection of the flow in a very small volume. The characteristic mixing time includes macromixing, which occurs on the scale of the vessel, mesomixing, which occurs on the scale of the turbulent eddies, and micromixing, which occurs on the scale of molecular diffusion in the stretching fluid lamellae [29]. The kinetic and mechanical energy input into the system is dissipated by viscous deformation of the fluid. The fluid is first distributed throughout the vessel by bulk mixing, followed by the

formation of daughter vortices which grow and engulf new fluid. Further deformation of the daughter vortices ultimately results in a lamellar structure. Molecular diffusion then eliminates regions of segregation [23]. A schematic representation of the flash nanoprecipitation process is shown in figure 1.2.

Flash nanoprecipitation is a promising technology for the encapsulation of hydrophobic drugs in a polymer based delivery vehicle. The overall goal of flash nanoprecipitation is to form stable nanoparticles that can be used for hydrophobic cancer drug delivery. The nanoparticle formulation conditions are an important parameter in achieving this goal. Ideally, stable sub-200 nm particles with a high drug loading will be made. Chapter 2 studies the effect of formulation conditions in FNP. Particle structure and mechanism of particle formation are also important as both relate to particle stability and the possible drug release profile. Nanoparticle structure is therefore studied in chapter 3. In order to translate the nanoparticles made by FNP to clinical use, some sort of post formulation treatment is necessary. One of the most commonly used methods is freeze drying. The effect of freeze drying on the nanoparticles is therefore examined in Chapter 4.

Chapter 2: Effect of formulation of nanoparticle size in flash nanoprecipitation

2.1. Introduction

Flash nanoprecipitation (FNP), developed by Prud'homme and coworkers [23, 24], is a promising technology for the encapsulation of hydrophobic drugs in a polymer based delivery vehicle. While FNP has been shown to make nanoparticles that are approximately 100 nm in size, there are several factors that can affect nanoparticle size and stability [27]. These factors include the materials being used to make the nanoparticle, the organic solvents being used, and the final concentration of the nanoparticle suspension.

The effect of the overall formulation in FNP was studied in order to determine the effect of formulation on particle size and stability. Two different types of block copolymer, each with two different molecular weights, were studied to explore the effect of formulation on particle size and stability. These two types of polymer were poly(ethylene glycol)-b-poly(lactic-co-glycolic acid) (PEG-b-PLGA) and poly(ethylene glycol)-b-poly(lactic acid) (PEG-b-PLA), whose structures are shown in figure 2.1. These block copolymers were chosen due to their biocompatibility and biodegrabability. PEG, PLA and PLGA are approved by the FDA and are widely used in food, cosmetics, and therapeutics [30, 31]. In flash nanoprecipitation, the hydrophobic PEG block forms the outer covering, or corona, of the nanoparticle. This PEG outer shell has been shown to reduce nonspecific interactions with proteins through its hydrophobicity and steric repulsion effects, reducing opsonization and thus helping the particles escape from the reticuloendothelial system [32, 33]. Adsorption of opsonins and plasma proteins on the particle surface can lead to internalization of nanoparticles into cells. Previous work

using PEG-b-PLGA nanoparticles smaller than 200 nm showed that the nanoparticles not only reduced uptake by the liver, but also prolonged drug retention time [34]. The "stealth" properties of PEG have been shown to increase circulation time and improved therapeutic efficacy of drugs using pegylated nanocarriers [33].

While nanoparticle drug delivery systems with particles between 5 and 250 nm show great potential to improve current disease therapies, there is no universally accepted standard for nanoparticle size to utilize the EPR effect. Rapid renal clearance of nanoparticles during systemic delivery is a critical issue for these systems. Along with surface composition, particle size is a key factor in the biodistribution of long-circulating nanoparticles and achieving therapeutic efficacy [33]. Bisht et al. [15] claimed that nanoparticles in the 10-100nm size range were able to deliver drugs most efficiently and facilitated long circulation time in the blood and higher uptake of drug in the tumor. However, there is a limit, as particles smaller than 20 nm cannot be prevented from renal clearance [35]. Lee et al. [36] studied the effect of nanoparticle size on the intratumoral uptake of block copolymer micelles (BCM). In their case, they made poly(ethylene glycol)-b-poly(caprolactone) (PEG-b-PCL) BCM's of 25 nm and 60 nm. They determined that the 25 nm particles cleared rapidly from the plasma compared to the 60 nm particles, resulting in an almost two fold increase in their total tumor accumulation. In another study by Fang et al. [37], protein absorption on small (80 nm) pegylated nanoparticles was compared to the same nanoparticle formulation with larger particle sizes (171 and 243 nm). Protein absorption on the small 80 nm particles was much less than for the larger particles, which was also confirmed with the analysis of nanoparticle

uptake by macrophages and blood clearance kinetics. These studies have indicated that tunable particle size is important for achieving effective targeted delivery.

In this work, two hydrophobic small molecules were used as the drug model: tetramenthoxysilicate and β-carotene (shown in figure 2.1). In previous studies [27], the water/octanol partition coefficient (logP) calculated by ACD/Chemsketch (Freeware download) [38] was correlated to nanoparticle stability. Zhu suggested that if the calculated LogP>~15, the nanoparticles showed good stability; if ~6<LogP<~9, the nanoparticles underwent fast Ostwald ripening and recrystallization; if LogP<~2, the drug was too soluble and nanoparticles could not be generated [27]. β-carotene and tetramenthoxysilicate were chosen as model drugs in this study due to their high hydrophobicity. The logP's for β-carotene and tetramenthoxysilicate as calculated by the ACDLogP software are 15.5 and 18.7, respectively. Based on this, both drug models should be sufficiently hydrophobic to form stable nanoparticles by FNP.

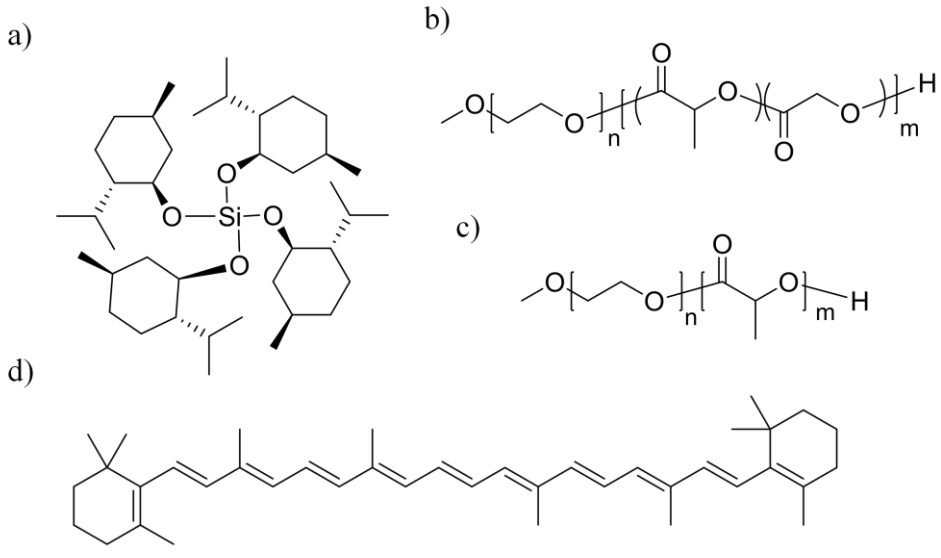

Figure 2.1: Chemical structures of the materials used for the formation of nanoparticles by flash nanoprecipitation. a) Tetramenthoxysilicate b) PEG-b-PLGA c) PEG-b-PLA d) β-carotene

In addition to the materials being used to form the nanoparticles, several other factors were altered in order to determine their effect on nanoparticle size and stability. The concentration of the dissolved solute in the organic phase, the ratio of polymer to drug model, the final dilution volume, and the organic solvent being used were all varied in order to study their effect on FNP. The goal of this study was to be able to understand and control the factors affecting particle size and stability. In doing so, we could provide a framework for the formulation of drug loaded nanoparticles with desirable properties for prolonged circulation and accumulation in tumors via the EPR effect.

2.2. Experimental section

2.2.1 PEG-b-PLGA synthesis

The PEG-b-PLGA used in this study was made by a controlled copolymerization of glycolide and lactide using poly(ethylene glycol) monomethyl ether (mPEG-OH) as a macroinitiator and an organic catalyst, 1,8-Diazabicyclo[5.4.0]undec-7-ene (DBU) as described by Qian et.al. [39]. This method gives a high conversion and narrow polydispersity index. Additionally, it eliminated metal containing catalysts, such as tin octoate, that are commonly used for synthesis but are less than ideal from a biological perspective [40].

mPEG-OH of molecular weight 5000 was purchased from Aldrich. The mPEG-OH was dried by dissolving in dry chloromethane and being stored overnight on oven-dried molecular sieves in an airtight culture tube. Glycolide was purchased from Altasorb and was purified by recystallization from THF, while D,L lactide was purchased from Altasorb and purified by recrystallization from toluene. Dichloromethane (CH_2Cl_2) and tetrahydrofuran (THF) were dried by passing through an activated alumina column.

1,8-diazabicyclo[5.4.0]-undec-7-ene (DBU) was purified by a one distillation from calcium hydride (CaH_2).

In order to synthesize the 5k-10k PEG-b-PLGA diblock copolymer, 450 mg of 5k mPEG-OH and 1000 mg of lactide were dissolved in 22 mL of dichloromethane in an oven dried round bottom flask containing a magnetic stir bar. 450 mg of glycolide was dissolved in 6 mL of THF and DBU was dissolved in CH_2Cl_2 at a concentration of 16.7 μL/mL. The glycolide solution was then taken up into a syringe, while the mPEG-OH and lactide solution were placed on a magnetic stir plate and vigorously stirred. The glycolide was placed on a syringe pump and DBU was then added to the PEG and lactide. Immediately after this addition, the glycolide was added to the reaction vessel at a rate of 0.6 mL/min. The tip of the syringe was submerged in the reacting vessel for the entire duration of the polymerization. At the end of the glycolide addition, 100 mg of benzoic acid was added to stop the polymerization. The reaction vessel was then brought over to a rotovap with a bath at approximately 40^{o}C and half of the solvent was boiled off. The polymer was then purified by dropwise addition to 150 mL of isoproponol. The isoproponol was then decanted off, the polymer redissolved in CH_2Cl_2 and repricipitated in isoproponol. The polymer was then dried in a vacuum oven overnight at 50^{o}C.

2.2.2. PEG-b-PLA synthesis

PEG-b-PLA was also made at ambient conditions in a fume hood as described by Qian et al [39]. A 5k mPEG-OH and CH_2Cl_2 solution (0.5g/mL) was dried over molecular sieves overnight. A 2.0 mL portion of this solution was then added to an 8.0 mL solution of dry CH_2Cl_2 in an oven dried, screw-capped glass reaction vessel. 10 μL of DBU was added and the resulting solution was stirred for 1 hr, at which point 150 mg of benzoic acid was added. The solution was concentrated and then added dropwise to an

excess of isoproponol. The isoproponol was then decanted off and the polymer was dried under vacuum at 50°C overnight.

2.2.3. PEG-b-PLA and PEG-b-PLGA characterization

Both the PEG-b-PLGA and PEG-b-PLA were verified by ^{1}H NMR the day after polymerization. The number average molecular weight was calculated by comparison of the ratio of the integrations of the methane and methylene signal of PLA and PGA redisdues vs the methylene signal of PEG residues. The known molecular weight of the PEG from the manufacturer enabled the calculation of the molecular weight of the PLGA and PLA blocks.

2.2.4. Particle synthesis

Nanoparticle formation was achieved by flash nanoprecipitation (FNP). Two different types of mixers, pioneered by Prud'homme et al. at Princeton University are available for FNP [41]. The confined impingement jet with dilution (CIJ-D) mixer impinges two streams before dilution, while the vortex mixer impinges four jets. Due to the ease of use, the two stream CIJ-D mixer was chosen for this study.

Figure 2.2: Image of the confined impingement jet (CIJ-D) mixer. The design dimensions for the mixer chamber were recommended by Johnson and Prud'homme [23]**.**

The CIJ-D mixer consists of two horizontal paths that lead to a small chamber in which the aqueous and organic streams are impinged. These are attached to two vertical openings on the top of the mixer where the two streams enter. After the two streams are impinged, they are collected from the outlet at the bottom of the mixer. Jing Han studied the effect of Reynolds number (Re) on nanoparticle size [42]. The Reynolds number is defined in equation 2.1.

$$Re = \frac{inertial\ force\ (= \rho V^2)}{viscous\ force\ (= \frac{\mu V}{L})} = \frac{\rho VL}{\mu} = \frac{\rho QL}{\mu A}$$

Eq. 2.1

ρ is the density of the fluid (kg/m^3), V is the mean fluid velocity (m/s), L is the stream inlet diameter, μ is the viscosity of the fluid (kg/m*s), A is the pipe cross sectional area (m^2), Q is the volumetric flow rate (m^3/s). In the case of the CIJ-D mixer, a modified form of the Reynolds number equation was used to account for the two streams involved in the mixing process. The modified form of the Reynolds number equation is given below in equation 2.2.

$$Re = \sum_{i=1}^{n} Re_i = \frac{d}{A}\sum_{i=1}^{n} \frac{\rho_i Q_i}{\mu_i} = \frac{4}{\pi d}\sum_{i=1}^{n} \frac{\rho_i Q_i}{\mu_i}$$

Eq. 2.2

In this case, d is the stream inlet diameter (m) and the subscript i denotes the ith inlet stream. Han determined that above a Re of 1000, the nanoparticles made by the CIJ-D mixer reached a critical size limit and size became independent of Re. Therefore, the CIJ-D mixer was used and mixing was accomplished by mixing the two streams by hand. An estimate of mixing by hand yielded a Re between 3600 and 6000, well above the Re=1000 limit. These Reynolds numbers correspond to a volumetric flow rate between

0.5 mL/s and 1 mL/s, while a Reynolds number of 1000 corresponds to a flow rate of 0.14 mL/s.

While the overall formulation was varied in this study, a standard mixing procedure is performed as follows. For the organic stream, 25 mg of a hydrophobic drug or drug model, along with 25 mg of an amphiphilic block copolymer was dissolved in 2.5 mL of an organic solvent (i.e. tetrahydrofuran (THF), acetone, dimethylformamide (DMF), etc.) (Sigma-Aldrich). This solution was then placed in a 3mL plastic, disposable syringe. A second syringe containing 2.5 mL of deionized water was also prepared. These two syringes were then attached to the two vertical openings on the CIJ-D mixer. A beaker containing 45.0 mL of deionized water (Sigma-Aldrich) was placed at the exit of the CIJ-D mixer. The exit stream outlet was submerged in the water. The two syringes were then pushed rapidly and simultaneously by hand to inject the liquids into the CIJ-D mixer at equal rates, where the two streams rapidly mixed before being diluted into the water bath at the bottom. This process resulted in a 0.1 wt% nanoparticle suspension in a 95:5 water: organic solvent solution.

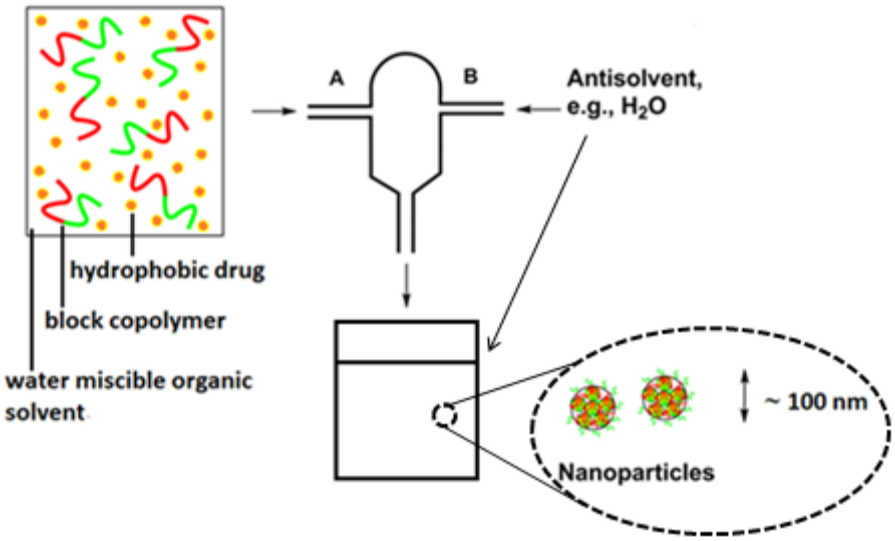

Figure 2.3: Schematic representation of the flash nanoprecipitation process.

2.2.5. Nanoparticle characterization

Nanoparticle size was determined by dynamic light scattering (DLS) using a ZetaPALS (Brookhaven Instruments, diode laser BI-DPSS wavelength of 659 nm). The light intensity correlation function was collected at 25°C and a scattering angle of 90°. DLS measures the time dependent fluctuations in the scattering intensity to determine the translational diffusion coefficient (D_T) and subsequently the hydrodynamic radius of the particles via the Stokes Einstein equation (eq. 2.3).

$$R_H = \frac{k_b T}{6\pi\eta_s D_T}$$

Eq. 2.3

R_H is the hydrodynamic radius, k_b is Boltzmann's constant, T is temperature, η_s is the solvent viscosity, and D_T is the translational diffusion coefficient.

Brownian motion is the random movement of particles due to bombardment by solvent molecules that surround them. In DLS, the speed at which the particles are

diffusing due to brownian motion is determined by measuring the rate at which the intensity of scattered light fluctuates when detected using a suitable optical arrangement. The rate at which these fluctuations occur will depend on the size of the particles. The dynamic information in DLS is derived from an autocorrelation of the intensity trace for the experiment. The correlator will contruct the correlation function of the scattered intensity and the particle size can then be obtained from the correlation function using various algorithms [43]. These include cumulants, CONTIN, and REPES. Cumulants fits a single exponential to the correlation function to obtain the mean size and an estimate of the width of the distribution [44]. CONTIN fits a multiple exponential to the correlation function to obtain a distribution of particle sizes [43]. REPES, which stands for regularized positive exponential sum, yields a series of discrete particle diameters to represent the particle distribution [45].

In this work, the particle size reported is the intensity average size as determined by the method of cumulants. The intensity average size of the particles, d_I, as determined by DLS is given below in equation 2.3.

$$d_I = \frac{\sum n_i d_i^6}{\sum n_i d_i^5}$$

Eq. 2.3

n_i is the number of particles and d_i is the particle diameter.

For particles sizes determined by DLS, the reported value is the average of at least 3 DLS runs and the error bar represents the standard deviation in the values of the runs. The polydispersity index as determined by DLS is based on the second order fit of the autocorrelation function and gives an indication of the variance of the system [46]

In several cases, transmission electron microscopy (TEM) was used to characterize the morphology and size of the nanoparticles. An FEI Tecnai T12 microscope was used for characterization. TEM grids (Carbon Type-B, 200 mesh, Copper approx. grid hole size: 97 μm) and uranyl acetate were purchased from Ted Pella. A 2 wt% uranyl acetate solution was used to stain the nanoparticles for TEM. Approximately 5 μL of the nanoparticle suspension was placed on the TEM grid. The extra suspension was then tapped off, leaving a thin film on the grid. A small drop of the 2 wt% uranyl acetate solution was then placed on the TEM grid and allowed to sit for 2-3 minutes before being wicked away from the underside of the grid with a piece of Whatman No.1 filter paper. The staining procedure was then repeated and the sample was allowed to dry before being analyzed by TEM.

2.3. Results

2.3.1. Effect of amphiphilic block copolymer

The effect of the amphiphilic block copolymer used in flash nanoprecipitation was studied. Particles were made using β-carotene as the model drug due to its high hydrophobocity and 5k-5k PEG-PLA, 5k-10k PEG-PLA, 5k-10k PEG-PLGA, and 10k-10k PEG-PLGA as the amphiphilic BCP. All particles were made using a 50 wt% loading of β-carotene.

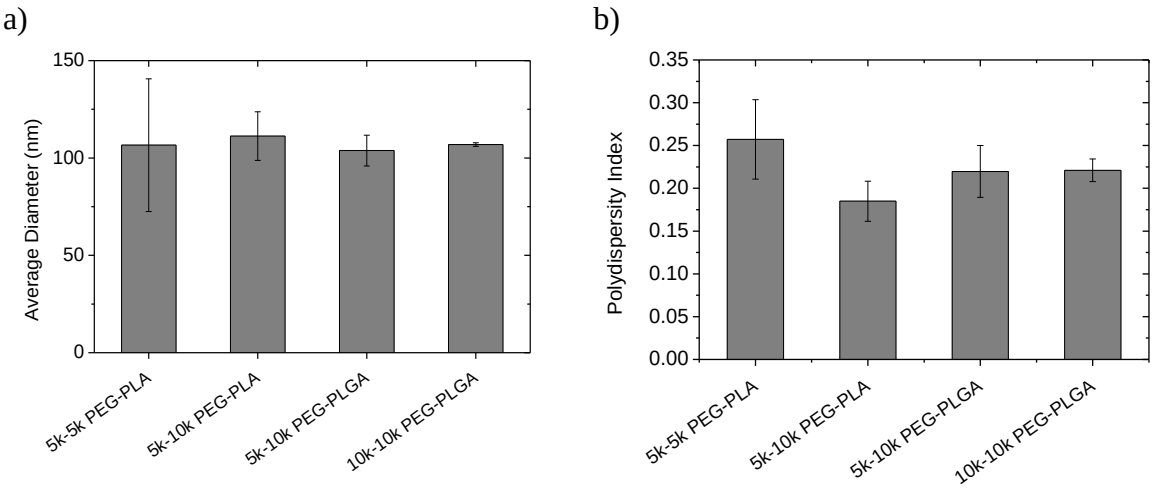

Figure 2.4: Effect of amphiphilic block copolymer on a) nanoparticles size and b) polydispersity index during flash nanoprecipitation. All particles were made using a 50% loading of β-carotene as the hydrophobic drug model and particle size and polydispersity were determined by DLS.

For all of the block copolymers used, the nanoparticles were in the correct size range to utilize EPR effect. All four BCP's made particles that were in the 100 to 110 nm range, as shown in figure 2.4. Additionally, the particles were all stable in suspension for a period of at least 72 hours. The polydispersity indices varied between 0.19 for 5k-10k PEG-b-PLA and 0.27 for 5k-5k PEG-b-PLA. The morphology of the nanoparticles was determined by TEM, as shown in figure 2.5.

a) b)

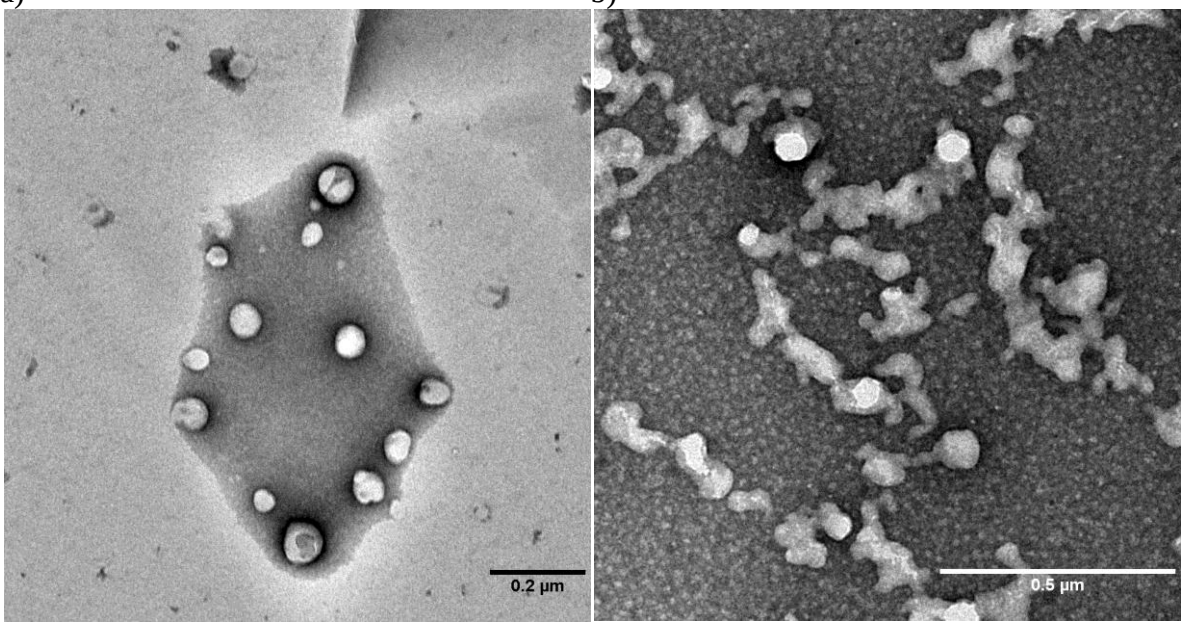

Figure 2.5: TEM images of particles made by flash nanoprecipitation. Particles were made using β-carotene as the model drug and a)10k-10k PEG-b-PLGA b) 5k-5k PEG-b-PLA as the block copolymer

For the case of the 10k-10k PEG-b-PLGA nanoparticles, the particles appear spherical and around 100 nm in diameter, confirming the size determined by DLS. However, the 5k-5k PEG-b-PLA nanoparticles appeared to have fused together leading to large deformed aggregates. However, the individual particles appear in agreement with the DLS value of ~100nm.

2.3.2. Effect of solute concentration in the organic phase

The effect of solute concentration in the organic phase for FNP was studied. In this case, tetramenthoxysilicate was used as the model drug and a 5k-10k PEG-b-PLGA was used as the amphiphilic block copolymer. The total concentration of dissolved solute was varied, while the mass ratio of the two components was kept constant at 50:50. In figure 2.6, it is clear that there was little to no change in particle size with the change in concentration.

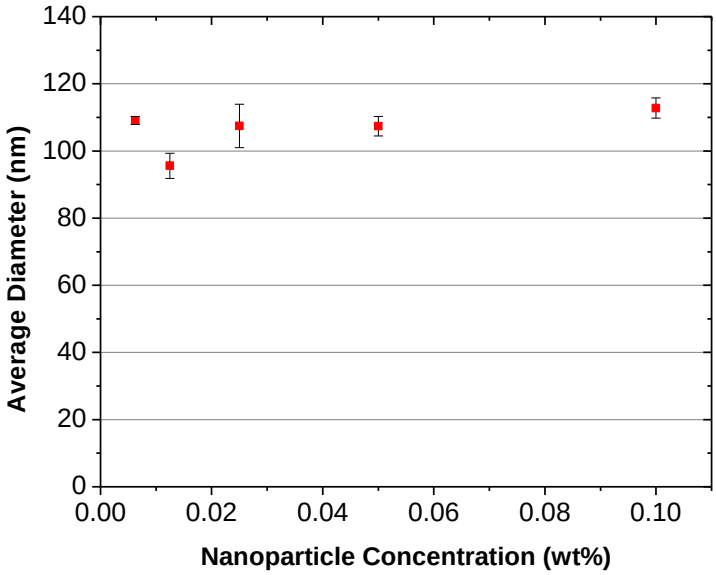

Figure 2.6: Effect of solute concentration on nanoparticle size. All particles were made using 5k-10k PEG-b-PLGA and tetramenthoxysilicate. The final concentration was varied by changing the amount of polymer and drug model dissolved in the organic phase while the final dilution was kept constant.

2.3.3. Effect of final dilution volume

The nanoparticle concentration in the final suspension was varied by altering the final dilution volume in FNP. All particles were made using 5k-10k PEG-b-PLGA as the amphiphilic BCP, β-carotene as the hydrophobic drug model, and THF as the water miscible organic solvent. The final particle solution was varied between 0.1 wt% and 1 wt%. The final dilution had an effect on the size of nanoparticles made by FNP, as shown in figure 2.7. In addition, an increase in the concentration also led to rapid nanoparticle instability.

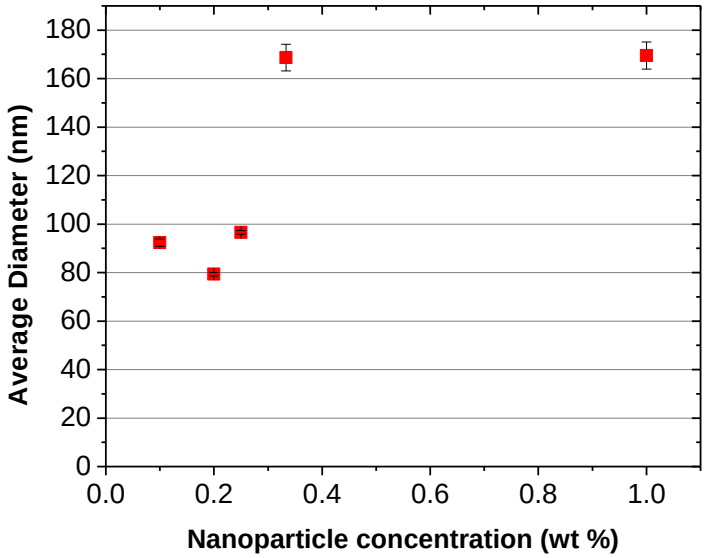

Figure 2.7: Effect of final dilution on final nanopartical size. All particles were made using 5k-10k PEG-b-PLGA and β-carotene. The nanoparticle concentration was varied by changing the final dilution volume while keeping the total amount of polymer and β-carotene constant.

2.3.4. Effect of drug loading

The ratio of 5k-10k PEG-b-PLGA to tetramenthoxysilicate was varied in FNP to determine its effect on particle size. At lower ratios of polymer to tetramenthoxysilicate, we would have a much higher loading, while at higher ratios there is a much lower loading. While the ratio of the two solutes was varied, the total concentration of solute dissolved in the organic phase (acetone) was kept contant. For example, a 50:50 mixture contained 25 mg of block copolymer and 25 mg of tetramenthoxysilicate dissolved in 2.5 mL of acetone, while a 30:70 mixture contained 15 mg of BCP and 35 mg of tetramenthoxysilicate. The ability to control particle size is important for the passive targeting of nanoparticles via the EPR effect. In addition, small, stable particles with a high drug loading are desirable as less excipient is required for their delivery. As the ratio of PEG-b-PLGA to tetramenthoxysilicate was increased, nanoparticle size decreased, as shown in figure 2.8. While particles made using only tetramenthoxysilicate were

attempted, their rapid precipitation resulted in the mixer jamming and no particles being made

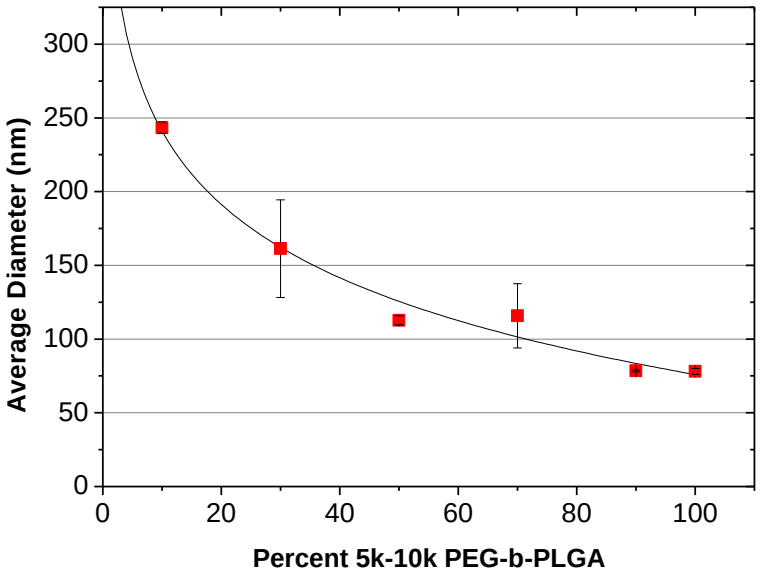

Figure 2.8: Effect of ratio of 5k-10k PEG-b-PLGA to tetramenthoxysilicate in FNP. The ratio of the polymer and drug model were varied while keeping the total concentration of dissolved solute constant.

2.3.5. Effect of organic solvent

The effect of the organic solvent on nanoparticle formation was studied. Particles were made using acetone, tetrahydrofuran (THF), and dimethylformamide (DMF) as the organic solvent. Particles were made by FNP using 5k-10k PEG-b-PLGA only and no drug or drug model. Particles made using THF were the largest, while those made using acetone as the organic solvent were the smallest as shown in figure 2.9.

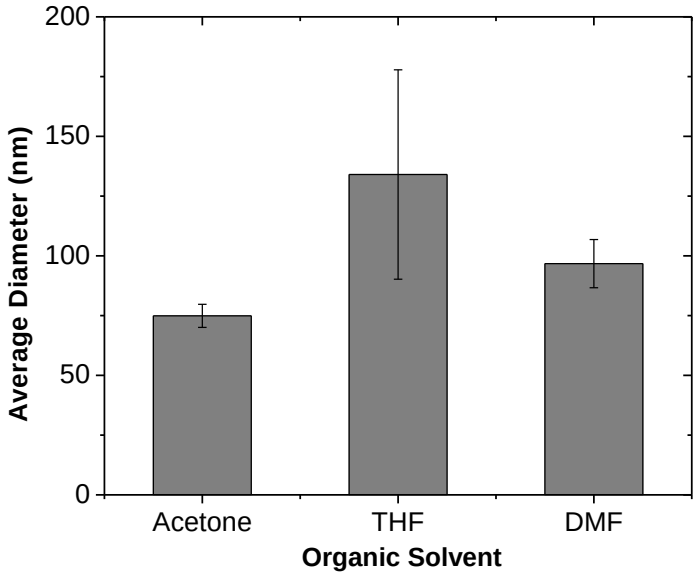

Figure 2.9: Effect of solvent on 5k-10k PEG-b-PLGA only nanoparticles made by FNP.

2.4 Discussion

In this study, the nanoparticle formulation was varied in order to determine its effect on nanoparticle size and stability. The goal of drug loaded nanoparticle made by FNP is to produce stable nanoparticles that can circulate in vivo for long periods and accumulate in tumors via the EPR effect. In order to do this, nanoparticles with a tunable size and long term stability are desirable. In the following section, the effect of varying nanoparticle formulation on nanoparticle size and stability is discussed.

2.4.1. Choice of block copolymer

The choice of block copolymer did not appear to have any effect on nanoparticle size. However, TEM imaging indicated a difference in nanoparticle morphology. The 5k-5k PEG-b-PLA particle appeared fused together as compared to the spherical 10k-10k PEG-b-PLGA particles, shown in figure 2.5. While the PEG-b-PLA particles appeared to be stable over time in suspension, the addition of the heavy metal salt (uranyl acetate ($UO_2(CH_3COO)_2$-$2H_2O$)) used for staining likely could have lead to their destabilization. In previous work, Zhu showed that particles made with PEG-b-PLA by FNP using a

vortex mixer underwent rapid aggregation with the addition of salt [27]. If the particles were electrostatically stabilized, the addition of uranyl acetate would have neutralized the surface charge and triggered the aggregation of the PEG-b-PLA nanoparticles. The choice of block copolymer is therefore an important choice for the stabilization of nanoparticles, particularly when it comes to their exposure to a saline environment.

2.4.2. Effect of solute concentration

The effect of solute concentration in the organic phase was studied to determine its effect on nanoparticle size. In classic crystallization theory, phase separation occurs at the onset of supersaturation in order to reduce the free energy of the system. In solvent exchange precipitations where a dissolved solute is added to a large volume of non solvent, the supersaturation is often given by

$$S = \frac{c}{c_\infty}$$

Eq. 2.4

Here, c is the total mass of the solute divided by the final solution volume and c_∞ is the bulk solubility in the final solvent mixture [25]. It is important to note that this definition of supersaturation has no relationship to the actual thermodynamic driving force for many solvent exchange precipitations, which happens locally and changes over time. Mass transfer or mixing limitation may make the actual supersaturation that controls nucleation and growth orders of magnitude smaller than the average value. In the case of FNP, however, the effect of mass transfer and mixing limitations are minimized and this definition of supersaturation becomes important.

The relative kinetics of nucleation and growth dictate the quality of the final particle size distribution. In previous studies, Mahajan and Kirwan explored the

nucleation and growth kinetics of lovastatin at low and high supersaturations in the absence of mixing limitations by using a grid mixer with a quantified mixing time of 3 ms [47]. They found that the nucleation rate increased with increasing supersaturation. In addition, both the nucleation rate and growth rate underwent a distinct transition as supersaturation was increased. This transition corresponded to a transition from heterogenous to homogenous nucleation. With a high supersaturation, secondary nucleation was largely avoided and the formation of nuclei was favored prior to significant growth. Therefore, a change in the supersaturation should have an effect on the size of nanoparticles.

In the case of block copolymer protected nanoparticles, the competitive nucleation and growth model for nanoparticle formation would cause a change in supersaturation to have an effect on nanoparticle size. During nanoparticle formation, the nucleation starts as either a homogenous nucleation of the hydrophobic molecules, or as a heterogenous nucleation of the block copolymer and hydrophobic molecule. In the case of homogenous nucleation, the hydrophobic molecule would nucleate with itself, likely due to a higher supersaturation and therefore higher nucleation rate than the block copolymer. The polymers would then assemble on the surfaces of the particles and arrest particle growth. In the case of heterogenous nucleation, the hydrophobic sites on the block copolymers would serve as nucleation seeds. The particle growth would then stop when polymer aggregation was terminated by the confined effects of particle dilution and steric hindrance of the hydrophilic block of the copolymer. In either case, at higher supersaturation, more nucleation sites would be generated, which would lead to the formation of smaller nanoparticles [48].

Altering the solute concentration in the organic solvent had no effect on the size of tetramamenthoxysilicate loaded nanoparticles, as shown in figure 2.6. This is possibly due to the degree of supersaturation being high regardless of the solute concentration in the feed solution. While it is possible that changing the concentration could change the size of the nanoparticles produced, the process was limited by the solubility of the tetramenthoxysilicate in the organic solvent on the high end and the ability to obtain a reading by DLS at lower concentrations. In either case, controlling nanoparticle size by varying the solute concentration is not a feasible option for FNP with the materials tested.

2.4.3. Dilution volume

In order to produce stable nanoparticles, a final dilution is required after mixing. However, the effect of this dilution volume had not been previously studied. In addition to altering nanoparticle size, an increase in the final nanoparticle concentration could lead to easier post processing after nanoparticle formulation. Particles made between 0.1 wt% and 0.3 wt% were all relatively close in size and appearance, as shown in figure 2.7. However, further increases in concentration by changing the final dilution volume lead to both an increase in nanoparticle size and particle instability. Nanoparticles made at 1 wt% precipitated rapidly after mixing due to the large THF to water ratio. Therefore, changing the nanoparticle size and the final solution concentration by changing the final dilution volume is not a feasible option for the materials tested.

2.4.4. Ratio of polymer to drug

The drug loading in FNP was studied as a way of controlling nanoparticle size. The results indicated an increase in nanoparticle size with an increase in loading, as

shown in figure 2.8. The increase in particle size with a decrease in the PEG-b-PLGA to tetramenthoxysilicate ratio is in agreement with the theoretical results of Cheng et al. [49]. In their modeling experiment, they determined that varying the ratio of the organic molecule (drug) to the block copolymer was one variable that could be used to control nanoparticle size in FNP. Cheng determined that the reason for the particle size variation was due to the strong effect of the ratio of the organic aggregation number distribution. A large polymer to organic ratio would lead to a smaller organic aggregation number. In addition, since the organic tends to couple with aggregates already containing an organic, there are many polymer-only aggregates when the organic to polymer ratio is small. This would lead to a decrease in the average particle size since polymer only particles are smaller than those loaded with drug. The change in particle size is therefore likely due to a small change in loaded drug nanoparticle size and a smaller average size as the number of polymer only nanoparticles is increased. However, the average nanoparticle size as determined by DLS did indicate that the loading of nanoparticles could be used as a means to control nanoparticle size. Further studies need to be conducted in order to fully understand how this average size is being affected, whether it is by a change in the loaded nanoparticle size, an increase in the number of small polymer only nanoparticles, or a combination of both.

2.4.5. Organic solvent

The choice of organic solvent had an effect on the size of nanopartcles made from 5k-10k PEG-b-PLGA, as shown in figure 2.9. One possible cause of the difference in nanoparticle size is the difference in the time of mixing between the organic phase and

the aqueous phase. The time of mixing of the two phases is based on the inverse of the diffusion coefficient of the solvent in water, as shown in equation 2.5 [23].

$$\tau_m = \frac{(0.5\lambda_k)^2}{D}$$

Eq. 2.5

τ_m is the time of mixing between the two phases, λ_k is the Kolmogorov length scale or the smallest eddy dimension which is able to form in turbulence prior to the domination of viscous effects and a laminar flow microstructure, and D is the diffusion coefficient of the solvent in water. For the three organic solvents used, the diffusion coefficient of acetone in water at 20^{o}C was the highest, followed by DMF and Acetone. This resulted in acetone having the smallest mixing time, and as expected, the smallest nanoparticle size. THF and DMF were both larger than particles made using acetone but did not follow the expected trend. However, the diffusion coefficients for these two organic solvents in water are close so other effects, such as solubility, could cause the difference in nanoparticle size.

2.5. Conclusions

Formulation parameters in FNP play a role in nanoparticle size and stability. The effect of block copolymer, concentration, dilution volume, hydrophobic compound loading, and organic solvent were studied to determine their affect on nanoparticles made by FNP. The choice of block copolymer did relatively little to effect the size and stability of nanoparticles in solution made by FNP. However, TEM imaging revealed differences in nanoparticle morphology. An appropriate choice of block copolymer is therefore important for the production of stable nanoparticles.

The final concentration of the nanoparticle suspension was varied by both changing the dissolved solute concentration as well as the final dilution volume. No change in size was seen by changing the solute concentration. However, this was limited by both the solubility of the hydrophobic moieties in the organic solvent on the high end and the detection limit for analysis on the low end. Changing the final dilution volume showed a much larger change in nanoparticle size and stability. However, large changes in dilution volume resulted in nanoparticle instability. While the study indicated a large dilution volume is necessary to produce stable nanoparticles, the dilution step cannot be used as a means of controlling final nanoparticle size.

Varying the drug loading and organic solvent were both effective ways of controlling nanoparticle size in flash nanoprecipitation. However, there are limits to the effectiveness of these two methods. Further work needs to be done to determine the exact cause of the change in particle size with loading. Additionally, lowering the loading to make smaller particles negates the advantage of making particles with a high loading by FNP. Changing the organic solvent used in FNP also led to a change in the resulting nanoparticle size, but solubility limited the degree to which this could be applied.

It is clear that the formulation parameters in FNP are important for nanoparticle formulation. Variations caused changes in both nanoparticle size and stability. Many of these parameters are worth further study. In several cases, we were limited by the solubility of the hydrophobic molecules in the organic solvent. Different hydrophobic molecules, particulary those which are actual drugs, should be tested to determine the most optimum formulation parameter.

Chapter 3: Nanoparticle structure

3.1. Introduction

While flash nanoprecipitation (FNP) has been used to effectively produce drug loaded nanoparticles below 100 nm in size, the mechanism of particle formation is unclear. The mechanism of nanoparticle formation is important because it will enhance the ability to control nanoparticle size and directly relates to the particle internal structure. Several different hypotheses exist as to how the nanoparticles form in the FNP process. Zhu [27] hypothesized that particles resulted from the formation of molecular clusters that then aggregate to form nanoparticles, trapping both the hydrophobic block of the polymer and drug in the nanoparticle core along with some of the hydrophilic block. Cheng et al. [50], however, have a different hypothesis on how the nanoparticles form. They modeled the co-precipitation process of a hydrophobic active (organic) and amphiphilic block copolymer in the FNP process and they determined particles were formed by the hydrophobic drug aggregating with itself or onto the hydrophobic block of the copolymer, while the hydrophilic block of the copolymer stretched out into the antisolvent to stabilize the particle. The initial aggregation occurred on a time scale much faster than mixing, but the particles could continue to grow through polymer insertion if mixing was incomplete. This would result in larger particles with slower mixing times. The resulting particles would be micellar-like in structure, with all of the hydrophobic components trapped in the core and the hydrophilic ones stretching out into the non-solvent. This model is similar to that predicted by Prud'homme et al. [23, 28, 51]. The mechanism of nanoparticle formation and incorporation of hydrophilic blocks of the block copolymer into the nanoparticle is important because it may alter the rate of

drug release by facilitating diffusion through loosely packed hydrophilic water pockets in the core [52]. Figure 3.1 shows a representation of the FNP process, as well as the two possible mechanisms for nanoparticle formation.

a)

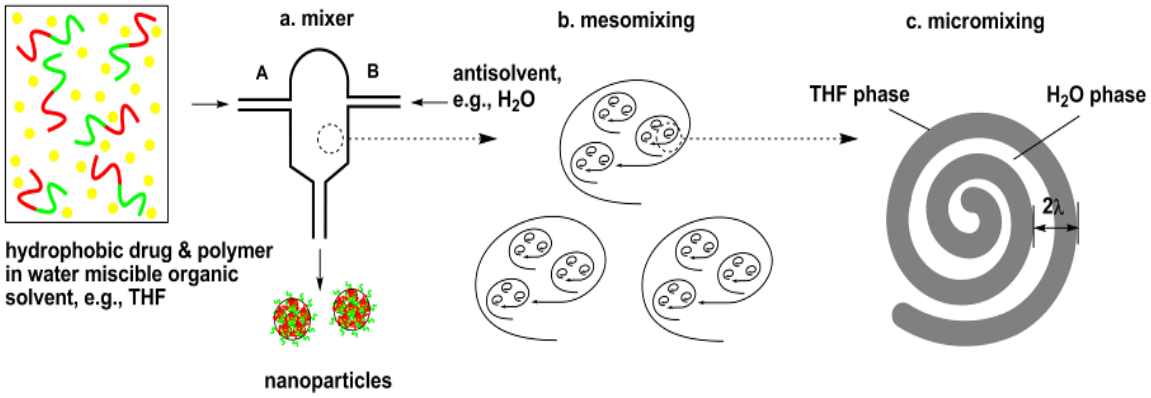

b)

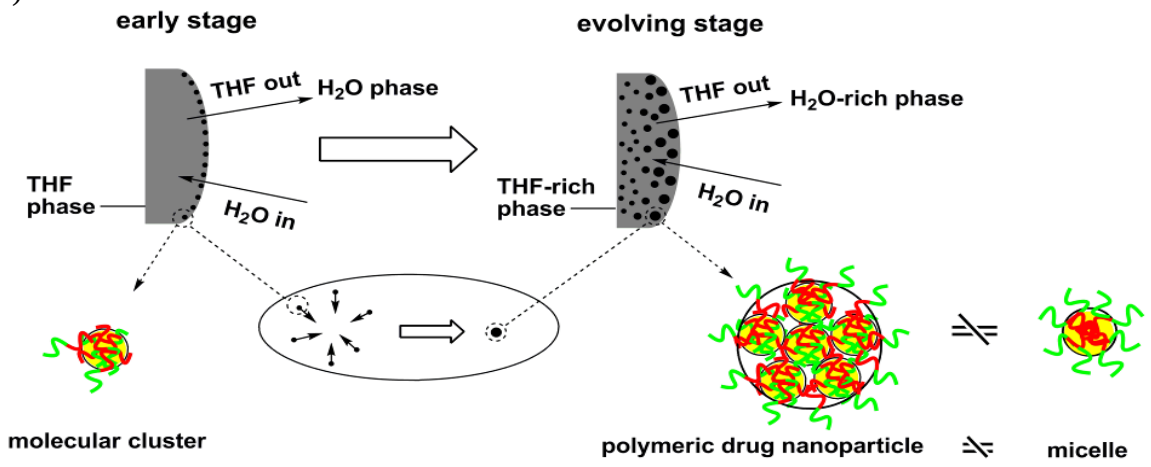

solvent shifting and nanoprecipitation

c)

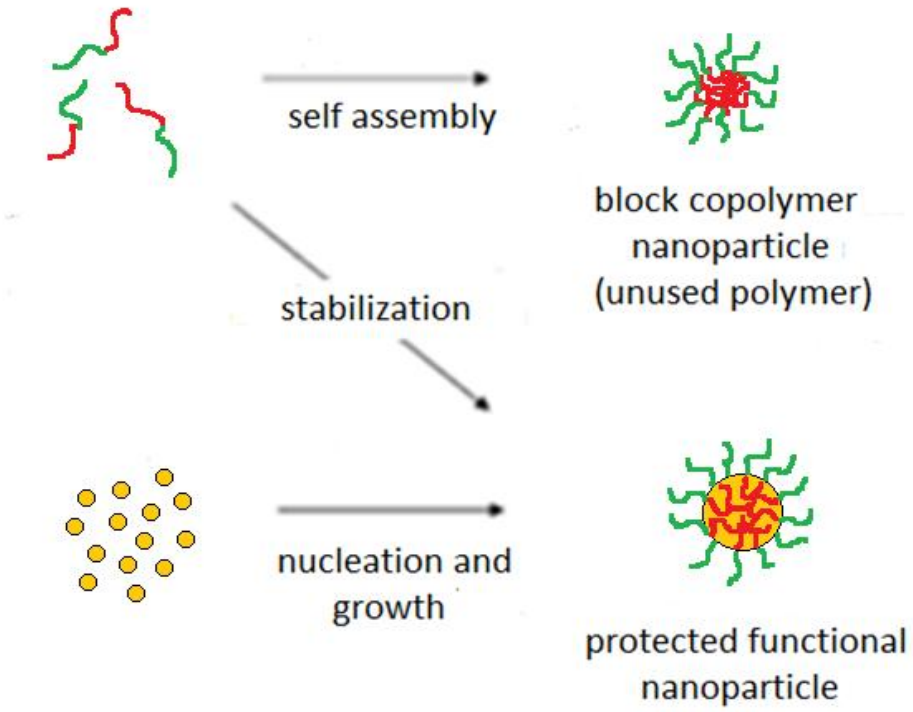

Figure 3.1: a) Schematic representation of the flash nanoprecipitation process to form block copolymer protected nanoparticles. Red represents the hydrophobic block of the copolymer, green the hydrophilic block, and yellow the hydrophobic drug [27] **b) Particle formation by nucleation and aggregation as predicted by Zhu, where molecular clusters come together to form nanoparticles** [27] **c) Nucleation and growth mechanism predicted by Cheng.**

Several experiments were performed to better understand the structure of the nanoparticle and the mechanism of nanoparticle formation. A 5k-10k PEG-b-PLGA was used as the amphiphilic diblock copolymer in all of the following studies, while the hydrophobic molecules used were tetramenthoxysilicate and a bis-triethylsilicate paclitaxel derivative [$(EtO)_3SiO$-PTX-$OSi(OEt)_3$], a more hydrophobic prodrug of paclitaxel. A prodrug is a pharmacological substance administered in an inactive form in vivo [53, 54]. During administration, the paclitaxel silicate prodrug can undergo

hydrolysis back to its active form in vivo [55]. These compounds were chosen since particles made previously using these compounds showed good stability. Both tetramenthoxysilicate and the paclitaxel prodrug had sufficiently high calculated logP's (18.7 and 18.4 [38], respectively) to prevent rapid Ostwald ripening, while 5k-10k PEG-b-PLGA produced β-carotene loaded nanoparticles that were stable for several weeks [27]. The chemical structures of bis-triethylsilicate paclitaxel, tetramenthoxysilicate, β-carotene and PEG-b-PLGA used in this study are shown in figure 3.2.

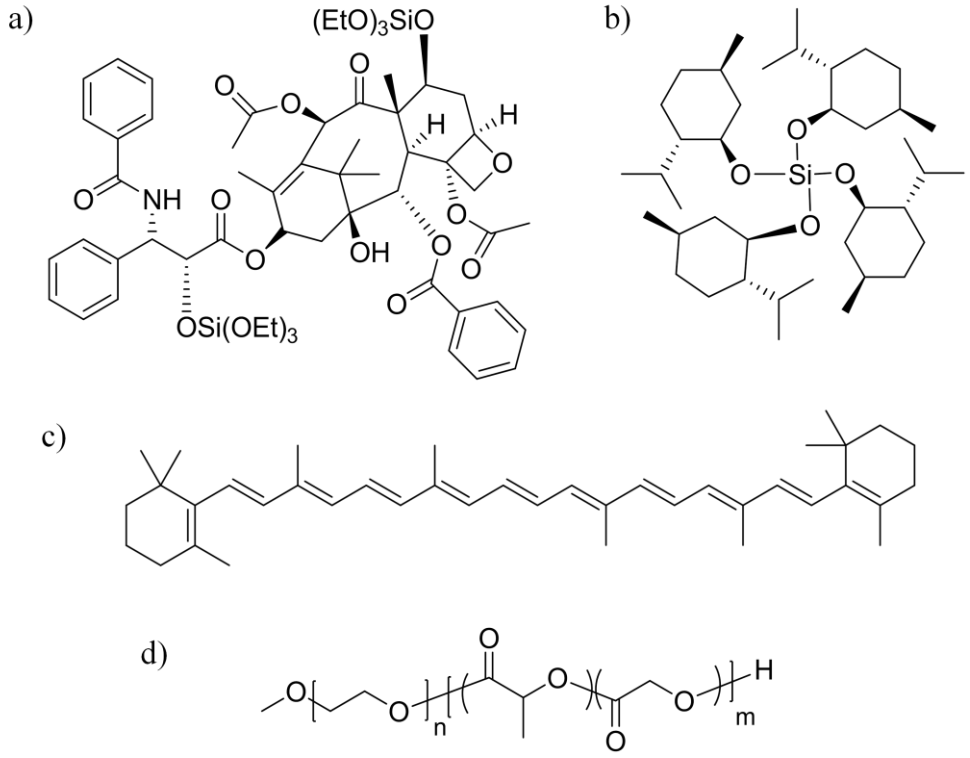

Figure 3.2 Structure of a) bis-triethylsilicate paclitaxel b) tetramenthoxysilicate c) β-carotene and d) PEG-b-PLGA used in this study. The bis-triethylsilicate paclitaxel is a prodrug of the anticancer drug paclitaxel.

3.2. Experimental section

3.2.1. PEG-b-PLGA synthesis

A 5k-10k PEG-b-PLGA was used as the amphiphilic diblock copolymer in this study. The polymer was synthesized at ambient conditions in a fume hood as described by Qian et al [39]. A more detailed description of the polymerization procedure, as well the block copolymer characterization, can be found in Chapter 2.

3.2.2. Particle synthesis

All particles were made via FNP using a Confined Impingement Jet (CIJ-D) mixer. The CIJ-D mixer consists of two streams that are rapidly mixed at high velocity in a confined space before being diluted in a large water bath. While the overall formulation is varied in FNP, a typical FNP procedure is outlined below. In one 3 mL syringe, 25 mg of an amphiphilic diblock copolymer as well as a suitable hydrophobic molecule was dissolved in 2.5 mL of tetrahydrofuran (THF). A second syringe containing 2.5 mL of deionized water was also prepared. These two syringes were then attached to two vertical openings on the top of the CIJ mixer. The two streams were then rapidly injected into the CIJ mixer at equal rates before being diluted into a 50 mL water bath.

3.2.3. Nanoparticle characterization

Nanoparticle size was determined by dynamic light scattering (DLS) using a ZetaPALS (Brookhaven Instruments, diode laser BI-DPSS wavelength of 659 nm). The light intensity correlation function was collected at 25°C and a scattering angle of 90°. The reported nanoparticle size is the intensity average size as determined by the method of cumulants. Cumulants fits a single exponential to the correlation function to obtain the

mean size and an estimate of the width of the distribution [44]. The reported size is also the average of three different batches of particles, each of which were analyzed by DLS three times. The reported error bars are the standard deviations from the nine total DLS runs.

Transmission electron microscopy (TEM) was used to characterize the morphology and size of the nanoparticles. An FEI Tecnai T12 microscope was used for characterization. TEM grids (Carbon Type-B, 200 mesh, Copper approx. grid hole size: 97 μm) and uranyl acetate were purchased from Ted Pella. In several cases, a 2 wt% uranyl acetate solution was used to stain the nanoparticles for TEM. Approximately 5 μL of the nanoparticle suspension was placed on the TEM grid. The extra suspension was then tapped off, leaving a thin film on the grid. A small drop of the 2 wt% uranyl acetate solution was then placed on the TEM grid and allowed to sit for 2-3 minutes before being wicked away from the underside of the grid with a piece of Whatman No.1 filter paper. The staining procedure was then repeated and the sample was allowed to dry before being analyzed by TEM. In the cases where osmium tetroxide was used to stain the sample, 5 uL of a 0.135M OsO_4 solution was added to 1 mL of the nanoparticle suspension. The particles were then allowed to stain for approximately 3 hrs. Following staining, a small drop of the suspension was added to a TEM grid and allowed to dry.

Cryogenic transmission electron microscopy (cryo-TEM) was also employed as a method of nanoparticle characterization and imaging and was performed by Han Seung Lee. Cryo-TEM samples were prepared in a controlled environment vitrification system maintained at 30^{o}C and 100% relative humidity. The samples were vitrified in liquid ethane at its freezing point. Samples were then viewed on a Tecnai G2 Spirit BioTWIN

TEM with the samples being kept at approximately -170^{o}C. Images were recorded using an Eagle 2k CCD camera.

3.3. Results and discussion

Several experiments were conducted in order to determine the structure of the nanoparticles, which could then be used to determine the method of nanoparticle formation. Nanoparticle size control studies were conducted by altering the formulation of the nanoparticles. In one case, the ratio of block copolymer to hydrophobic drug model was altered in order to determine the effect of loading on nanoparticle size. In this case, 5k-10k PEG-b-PLGA was used as the amphiphilic diblock copolymer, while tetramenthoxysilicate was used as the hydrophobic drug model. These structures are shown in figure 3.2. While the ratio of the two solutes was varied, the total concentration was kept constant. For example, a 50:50 mixture contained 25 mg of block copolymer and 25 mg of tetramenthoxysilcate dissolved in 2.5 mL of acetone, while a 30:70 mixture contained 15 mg of block copolymer and 35 mg of tetramenthoxysilicate.

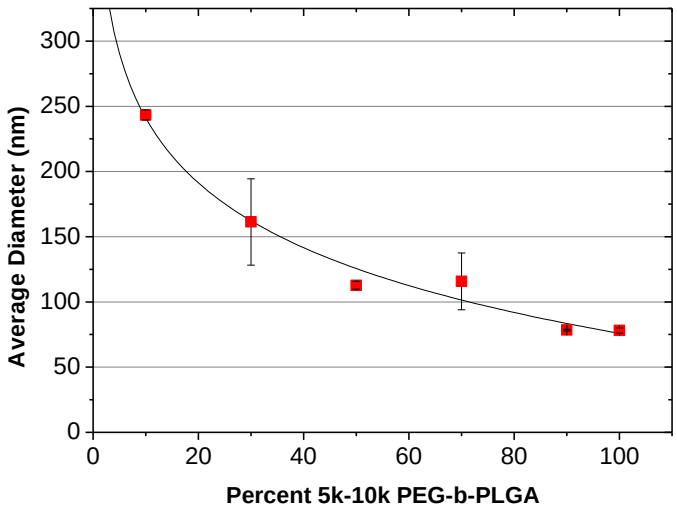

Figure 3.3: Particle diameter as a function of percent PEG-b-PLGA. All nanoparticles were made using 5k-10k PEG-b-PLGA as the amphiphilic block copolymer and tetramenthoxysilicate as the hydrophobic drug model. The total concentration was kept constant, with a total of 50 mg of block copolymer and tetramenthoxysilicate dissolved in acetone for each run.

The increase in particle size with a decrease in the ratio of PEG-b-PLGA to tetramenthoxysilicate, as shown in figure 3.3, is in agreement with the theoretical results of Cheng. The explanation for this change in size from a nucleation and growth point of view was due to a larger number of polymer only nanoparticles forming when small amounts of the drug were available to form nanoparticles. Since polymer only nanoparticles are smaller than those loaded with drug, the average particle size would be smaller when large numbers of polymer only nanoparticles were present. Additionally, at higher drug loadings, the tetramenthoxysilicate nucleation and growth was likely faster compared with polymer micellization. The tetramenthoxysilicate had a chance to form larger particles before the polymer arrested the growth of the particles. While the results agree with a nucleation and growth mechanism for nanoparticle formation, they do not give a conclusive answer about the mechanism of particle formation. Zhu's model for a nucleation and aggregation method of nanoparticle formation also agrees with these results. However, the change in particle size would be caused by smaller amounts of the hydrophobic drug or drug model being trapped in each particle as the ratio increased, as opposed to some large particles and many unloaded polymer only nanoparticles.

3.3.1 Particle imaging

Transmission electron microscopy (TEM) was explored as a way to determine the nanoparticle structure, and in turn the method of nanoparticle formation. We believed that by selectively staining the nanoparticle core, a core shell structure for the nanoparticle could be discerned that would support one of the two proposed formation mechanisms. For this study, a paclitaxel silicate prodrug, bis-triethylsilicate paclitaxel, was used for the hydrophobic drug and a 5k-10k PEG-b-PLGA was used as the

amphiphilic diblock copolymer. After the particles were made they were determined to be 120 nm by DLS with a polydispersity index of 0.07. Following formulation, the particles were stained in solution using a .135 M osmium tetroxide (OsO_4) solution. OsO_4 is a commonly used stain for imaging of polymers containing carbon-carbon double bonds [56]. By taking advantage of the carbon-carbon double bonds in the paclitaxel prodrug, the core of the nanoparticle could be selectively stained and provide contrast in the TEM. In this case, 5 uL of the OsO_4 solution was added to 1 mL of the nanoparticle suspension. The particles were then allowed to stain for approximately 3 hrs. Following staining, a small drop of the suspension was added to a TEM grid and allowed to dry. In addition to staining the particles with OsO_4, a second TEM sample was prepared using uranyl acetate to stain the particles.

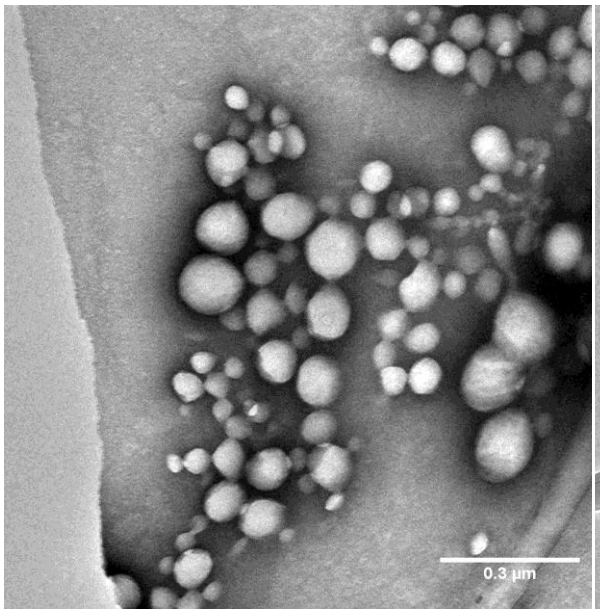

Figure 3.4: TEM image of 5k-10k PEG-b-PLGA/ bis-triethylsilicate paclitaxel nanoparticles stained with uranyl acetate

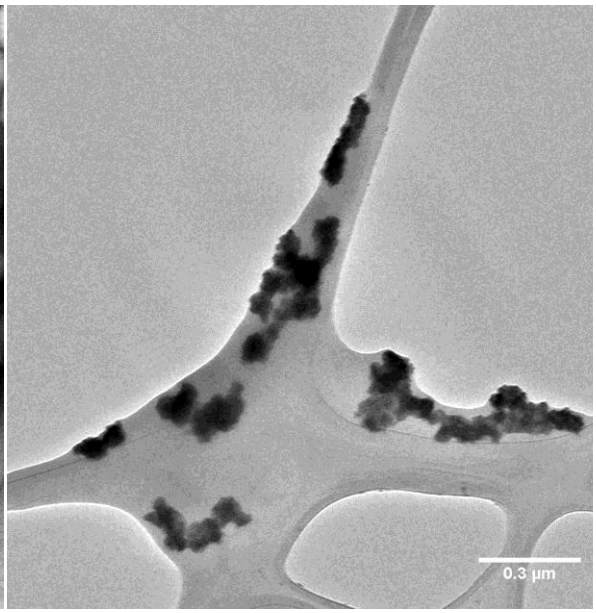

Figure 3.5: TEM image of 5k-10k PEG-b-PLGA/ bis-triethylsilicate paclitaxel nanoparticles stained with Osmium Tetroxide

A clear difference between the OsO_4 stained particles and the uranyl acetate stained particles was observed, as seen in figure 3.4 and 3.5. The uranyl acetate stained particles

appear to have a relatively broad distribution. One argument for a nucleation and growth model would be a bimodal distribution in particle size between the loaded and unloaded particles. While there is a distribution in nanoparticle size, there is no clear difference between what particles are loaded and unloaded. With the OsO_4 staining, no individual particles are visible. However, the dark areas in the image could be the selectively stained nanoparticle core. Combining the OsO_4 stain with the uranyl acetate staining should then indicate a difference between the loaded and unloaded nanoparticles and give an idea of the mechanism of nanoparticle formation.

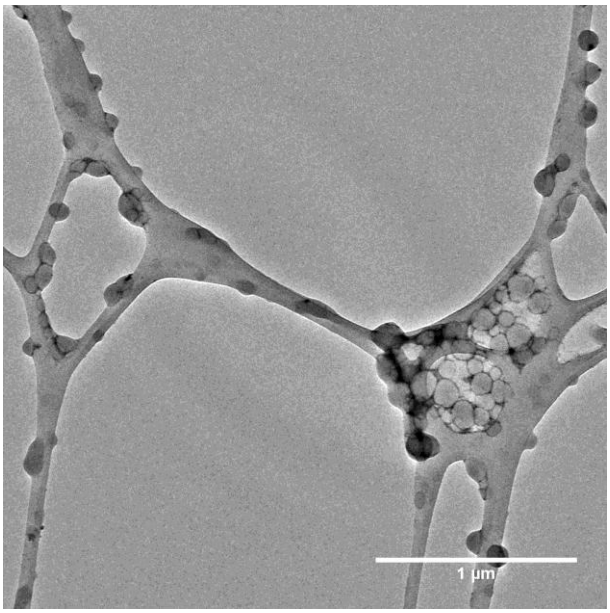

Figure 3.6: TEM image of 5k-10k PEG-b-PLGA/ bis-triethylsilicate paclitaxel nanoparticles stained with OsO_4 and uranyl acetate

Staining with OsO_4 showed no clear difference between what could be loaded and unloaded particles as seen in figure 3.6. While a nucleation and aggregation model would likely indicate particles with some drug in each of them, it is not clear that the drug loaded particles have been stained. Therefore, the dual staining technique did not provide

a clear understanding of the nanoparticle structure and mechanism of nanopartice formation.

3.3.2. Cryo-TEM imaging

Cryogenic transmission electron microscopy (cryo-TEM) was employed as a method of nanoparticle characterization and imaging. In cryo-TEM, the sample is vitrified before viewing, causing the nanoparticles to stay in their native conformation. In addition, heavy metal stains that could cause instability are not necessary and the drying process can be avoided.

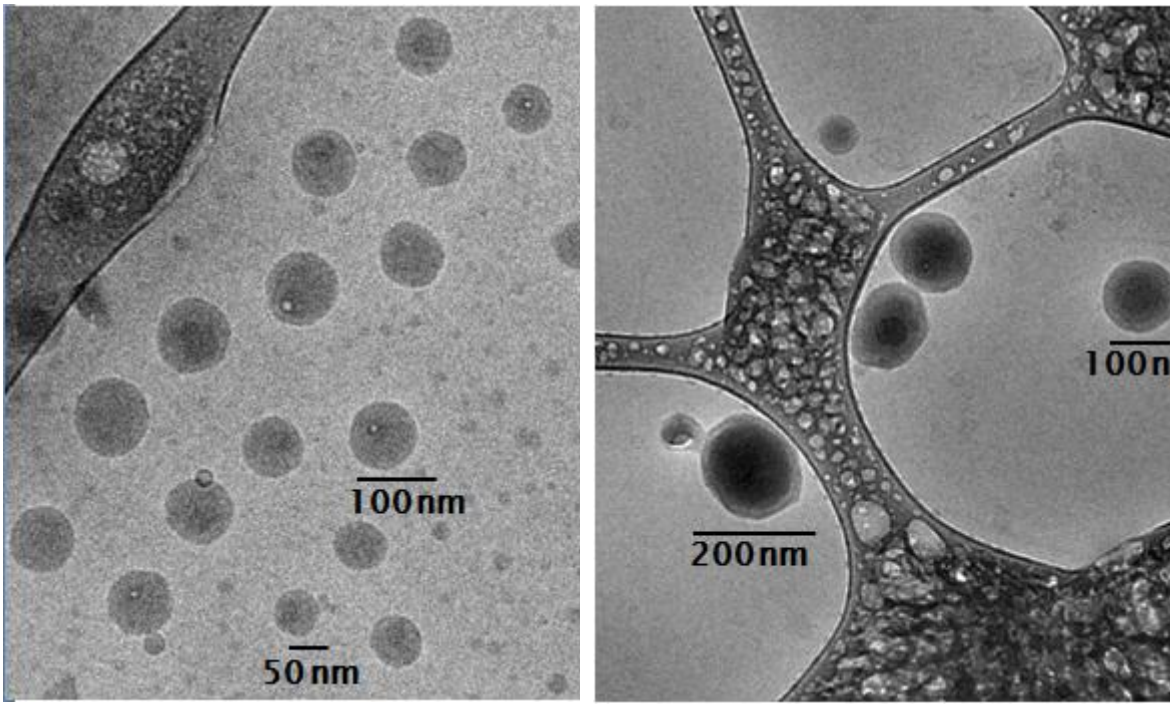

Figure 3.7: Cryo-TEM images of 5k-10k PEG-b-PLGA/bis-triethylsilicate paclitaxel nanoparticles. Cryo-TEM performed by Han Seung Lee.

The cryo-TEM images show many spherical particles in the 100 nm size range. In addition to these ~100 nm particles, many small particles are visible in the background. This bimodal particle distribution is indicative of a nucleation and growth mechanism of particle formation. The large 100 nm particles are likely the drug loaded

nanoparticles, while the small particles are polymer only micelles. In addition, the images reveal a core shell structure in the larger particles, with a dark core area and a lighter shell structure. The contrast is likely provided from the Si atom in the PTX-Si prodrug, causing the core of the particles to scatter the electron beam to a greater extent and therefore appearing darker in the TEM image. The core-shell structure of the nanoparticles along with a bimodal distribution in nanoparticle size as shown by cryo-TEM is a strong argument for the nucleation and growth mechanism of nanoparticle formation in FNP.

3.4 Conclusion

Flash nanoprecipitation is an effective way to produce hydrophobic drug loaded nanoparticles around 100 nm with relatively high drug loadings. However, the mechanism by which these particles form, as well as the nanoparticle structure, remain unclear. In this study, particle loading and microscopy techniques were evaluated in order to determine the likely method of particle formation, whether it be a nucleation and growth or a nucleation and aggregation mechanism. Particle size trends, as well as particle size distribution and structure as revealed by cryo-TEM support a nucleation and growth mechanism of particle formation.

In order to further elucidate the nanoparticle structure and mechanism of particle formation, further studies are required. While cryo-TEM appeared to indicate a core shell structure for the bis-triethylsilicate paclitaxel prodrug loaded nanoparticles, the chemical structure of the hydrophobic molecules did not allow for a large amount of contrast. In order to provide better contrast, a hydrophobic molecule containing a more electron dense atom, such as iodine, must be used. Nanoparticles containing

triiodophenol as the hydrophobic molecule were attempted. However, triidophenol was not sufficiently hydrophobic (calculated logP=3.9) to form stable nanoparticles.

Additionally, the particle size studies using varying loadings of tetramenthoxysilicate were based on the particle size determined using DLS. While the trend in particle size seems to support a nucleation and growth model for particle formation, the results are inconclusive. Cryo-TEM should be employed to analyze the nanoparticle made at different loading. In doing so, we may be able to determine whether the increase in nanoparticle size with higher drug loading is due to larger nanoparticle cores or due to particle aggregation caused by insufficient steric stabilization on the outside of the particles.

Chapter 4: Freeze drying of polymer nanoparticles made by flash nanoprecipitation

4.1 Introduction

Drug solubility is one of the most significant challenges when it comes to designing drug delivery systems [1]. Nano-scale drug delivery systems show great promise for the delivery of insoluble drugs, particulary anticancer drugs due to passive targeting via the enhanced permeation and retention (EPR) effect [7, 57]. Flash nanoprecipitation (FNP), developed by Prud'homme and coworkers, is one promising technology for the encapsulation of hydrophobic drugs in a polymer based delivery vehicle [23, 24]. FNP has been shown to make nanoparticles of approximately 100 nm in diameter, which is ideal for the utilization of the EPR effect. Additionally, when a 5k-10k poly(ethylene glycol)-b-poly(lactic-co-glycolic acid) (PEG-b-PLGA) was used as the amphiphilic diblock copolymer and β-carotene as the drug model, stable nanoparticles were produced and particles remained stable in suspension for a period of 10 days [27].

While the use of 5k-10k PEG-b-PLGA and β-carotene for the formation of nanoparticles by FNP lead to the formation of nanoparticles stable in suspension over a short period, longer term storage in suspension remains one of the major obstacles that limits the use of nanoparticles as a drug delivery system. Both physical instability (particle fusion/aggregation) and chemical instability (drug leakage of nanoparticles, hydrolysis of the polymer material forming the nanoparticles, and chemical reactivity of the medicine during storage) severely limit the use of hydrophobic drug loaded nanoparticles when stored in suspension [58]. While these instabilities are potentially advantageous during actual nanoparticle delivery, they are not ideal during storage. For particles made by FNP, organic solvents, such as tetrahydrofuran (THF), also must be

removed from the suspension before particles can be used in a clinical application. Additionally, the concentration of the nanoparticles in the suspension may need to be altered in order to achieve the optimum therapeutic effect. For these reasons, it is clear that some sort of post formulation treatment is necessary for translation to clinical use.

Freeze drying, also known a lyophilization, is considered to be one the best processes for treating nanoparticle suspensions after formulation [59]. Freeze drying is a commonly used process which allows the particles to be converted into solids of sufficient stability and storage [60]. Freeze drying is an industrial process that consists of removing water from a frozen sample by sublimation and desorption under vacuum. While freeze drying is an effective way of removing water from the system, there are several issues involved with the process that can affect the nanoparticle system. During the freezing and drying steps, various stresses are generated that can affect the system. These include both mechanical stresses from freezing as well as stresses due to dehydration. For this reason, some sort of protectant is normally added to the formulation to protect the nanoparticles from the freezing and desiccation stresses [61].

There are several important goals that should be aimed for when freeze drying nanoparticulate systems. Long term stability of the formulation, conservation of the physical and chemical characteristics of the freeze dried product (an unmodified nanoparticle size and drug entrapment), and a rapid and low energy reconstitution time will help to improve the performance of the lyophilized nanoparticles [61]. Process parameters such as colloidal concentration, freezing rate and temperature, cryoprotectant type and concentration, drying time and temperature can all affect the ease to which a dry powder can be suspended back to its original particle size.

In this study, the effect of freezing and freeze drying with and without the use of cryoprotectants on nanoparticles made by FNP was studied. β-carotene was used as a drug model, while 5k-10k PEG-b-PLGA was used as the amphiphilic block copolymer. β-carotene, a precursor for vitamin A, was used as a model drug because of its high hydrophobicity (calculated logP=15.5, ACDLogP software) [38]. Previous work by Zhu [27] suggested that if the calculated logP>15, the nanoparticles were stable in suspension for a period of at least 10 days. The high hydrophobicity ensured that the nanoparticles were relatively stable in terms of recrystallization and Ostwald ripening. PEG-b-PLGA was chosen because it has previously been shown to effectively stabilize β-carotene nanoparticles [27]. Both PEG and PLGA are approved for use by the FDA and are widely used in food, cosmetics and therapeutics due to their biocompatibility and biodegradability [30,31]. The hydrophilic PEG outer shell of the nanoparticles can reduce protein opsonization on the particle surface and help the particles escape from the reticuloendothelial system after intravenous administration [34]. In addition to using β-carotene as the drug model, nanoparticles made using a prodrug of paclitaxel (PTX) were made to determine the effect of freeze drying on nanoparticles made using a different drug. The chemical structures of the bis-triethylsilicate paclitaxel (the more hydrophobic prodrug of paclitaxel), PEG-b-PLGA, and β-carotene are shown in figure 4.1.

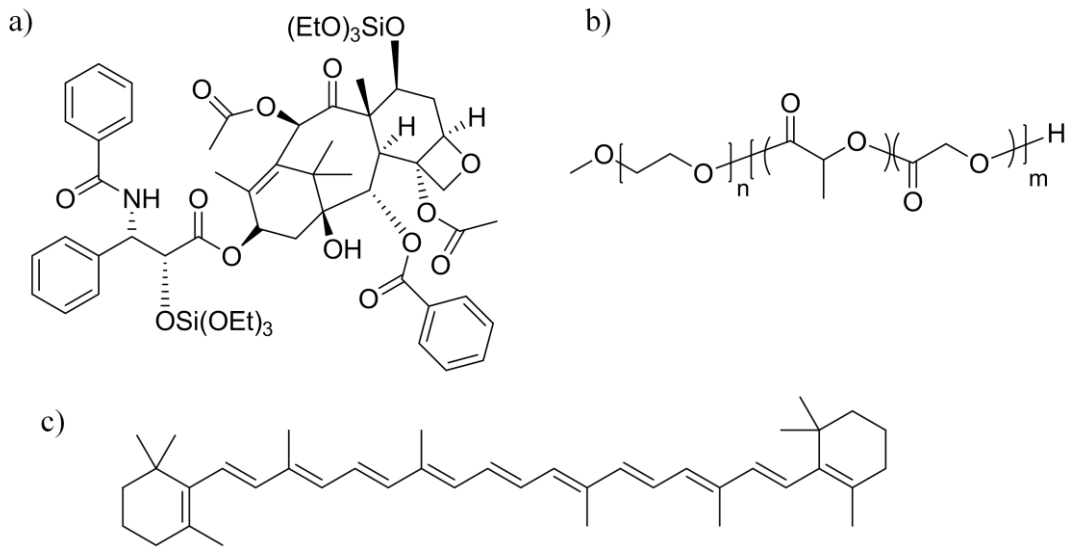

Figure 4.1: Chemical structures of a) bis-triethylsilicate paclitaxel, a more hydrophobic prodrug of paclitacel, b) PEG-b-PLGA, and c) β-carotene.

4.2 Experimental section

4.2.1. PEG-b-PLGA and PEG-b-PLA synthesis

A 5k-10k PEG-b-PLGA was used as the amphiphilic diblock copolymer in this study. The polymer was synthesized at ambient conditions in a fume hood as described by Qian et al [39]. A more detailed description of the polymerization procedure, as well the block copolymer characterization, can be found in Chapter 2.

4.2.2. Particle synthesis

All nanoparticles made in this study were made using FNP and a confined impingment jet (CIJ-D) mixer. The CIJ-D mixer, developed by Prud'homme et al. at Princeton University, impinges two streams at high velocity in a confined space before dilution in a water bath. A standard formulation for the FNP process is performed as follows. For the organic stream, 25 mg of a hydrophobic drug or drug model, along with 25 mg of an amphiphilic block copolymer, were dissolved in an organic solvent, such as tetrahydrofuran (THF). In this study, unless otherwise noted, all samples were made

using THF (Sigma-Aldrich). This solution was then placed in a disposable 3 mL plastic syringe syringe. A second syringe containing 2.5 mL of deionized water (Sigma-Aldrich) was also prepared. These two syringes were then attached to the two vertical openings on the CIJ-D mixer. A beaker containing 45.0 mL of deionized water was placed at the exit of the CIJ-D mixer, with the exit stream being completely submerged in water. The two syringes were then rapidly injected into the CIJ-D mixer at equal rates, where the two streams were rapidly mixed before being diluted in a water bath. This process resulted in a 0.1 wt% suspension in a 95:5 water:organic solvent solution.

4.2.3. Differential scanning calorimetry

Differential scanning calorimetry (DSC) (TA Instruments Q1000) was used to determine how the addition of cryoprotectants affected to freezing of water. Approximately 15 μL of either a 2 0wt% solution of sucrose or Pluronic F68 was transferred to a hermetically sealed aluminum DSC pan. The samples were first cooled at 10°C/min to a temperature of -80°C and then heated at 10°C to a temperature of 60°C. The data shown in figures 4.6 and 4.9 is upon heating of the sample from -80°C to 60°C.

4.2.4. Freeze drying

In this study, all nanoparticle suspensions were frozen in liquid nitrogen for at least 15 minutes prior to either freeze drying or thawing. In the cases that cryoprotectants were used, the cryoprotectant was first dissolved at the appropriate concentration in the suspension before freezing took place. All samples were places in 15 mL plastic centrifuge tubes. After freezing, these samples were transferred to glass vessel that was then connected to a dual stage rotary vane vacuum pump. A vacuum was pulled on the samples for at least 24 hours, at which point they were removed from the freeze dryer and

transferred to a -4°C freezer for storage. Figure 4.2 shows a diagram of the freezing and freeze drying processes.

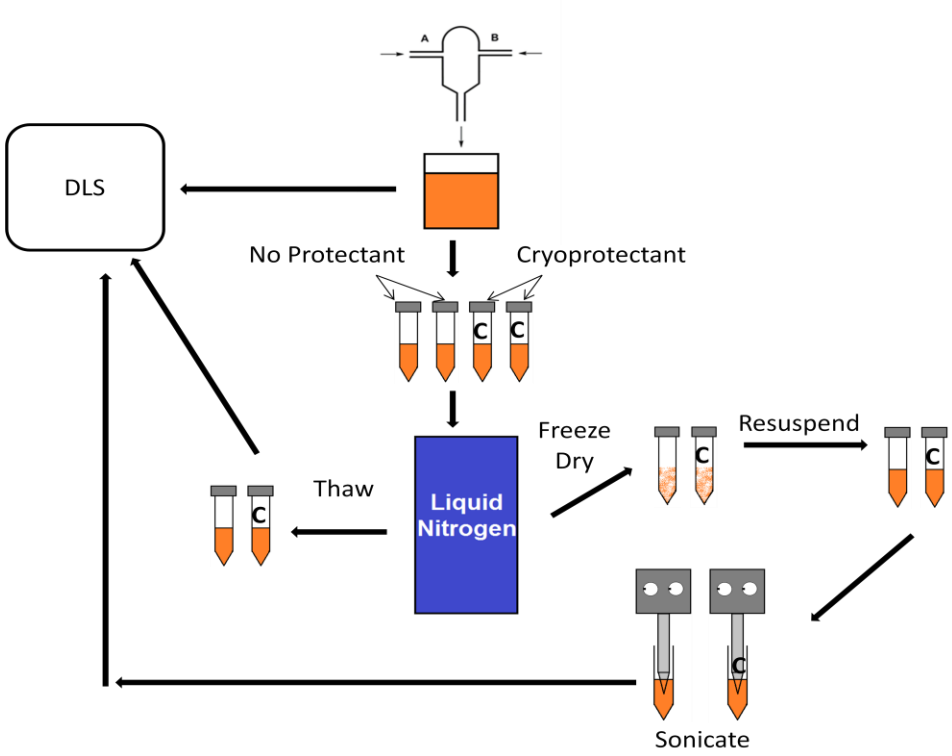

Figure 4.2: Diagram of the freeze drying and redispersion processes. In several cases, a freeze thaw process was used.

4.2.5. Nanoparticle characterization

Nanoparticle size was determined by dynamic light scattering (DLS) using a ZetaPALS (Brookhaven Instruments, diode laser BI-DPSS wavelength of 659 nm). The light intensity correlation function was collected at 25°C and a scattering angle of 90°. In this work, the particle size reported is the intensity average size as determined by the method of cumulants. The intensity average size of the particles, d_I, as determined by DLS is given below in equation 4.1.

$$d_I = \frac{\sum n_i d_i^6}{\sum n_i d_i^5}$$

Eq. 4.1

n_i is the number of particles and d_i is the particle diameter.

For particles sizes determined by DLS, the reported value is the average of at least 3 DLS runs on single batch and the error bar represents the standard deviation in the values of the runs.

In several cases, transmission electron microscopy (TEM) was used to characterize the morphology and size of the nanoparticles. An FEI Tecnai T12 microscope was used for characterization. TEM grids (Carbon Type-B, 200 mesh, Copper approx. grid hole size: 97 μm) and uranyl acetate were purchased from Ted Pella. A 2 wt% uranyl acetate solution was used to stain the nanoparticles for TEM. Approximately 5 μL of the nanoparticle suspension was placed on the TEM grid. The extra suspension was then tapped off, leaving a thin film on the grid. A small drop of the 2 wt% uranyl acetate solution was then placed on the TEM grid and allowed to sit for 2-3 minutes before being wicked away from the underside of the grid with a piece of Whatman No.1 filter paper. The staining procedure was then repeated and the sample was allowed to dry before being analyzed by TEM.

Cryogenic transmission electron microscopy (cryo-TEM) was also employed as a method of nanoparticle characterization and imaging. In cryo-TEM, the sample is vitrified before viewing, causing the nanoparticle to stay in its native conformation. Heavy metal stains that could cause instability are not necessary and the drying process can therefore be avoided. Cryo-TEM samples were prepared in a controlled environment vitrification system maintained at 30^{o}C and 100% relative humidity. The samples were vitrified in liquid ethane at its freezing point. Samples were then viewed on a Tecnai G2

Spirit BioTWIN TEM with the samples being kept at approximately -170^{o}C. Images were recorded using an Eagle 2k CCD camera.

4.3 Results and discussion

4.3.1. Freeze-thaw study

During the freezing process, the nanoparticles in the suspension undergo mechanical stresses that could have significant effects on nanoparticle redispersibilty and stability [61]. As the water in the samples freezes and turns into ice, the nanoparticles are expelled into areas of higher and higher concentration, as shown schematically in figure 4.3. It is well known that there is a phase separation in the sample during freezing into ice and a cryo-concentrated solution, which in the case of nanoparticle suspensions consists of the nanoparticles and any other components of the formulation [62]. Such a high concentration of the particulate system can induce aggregation, and in some cases

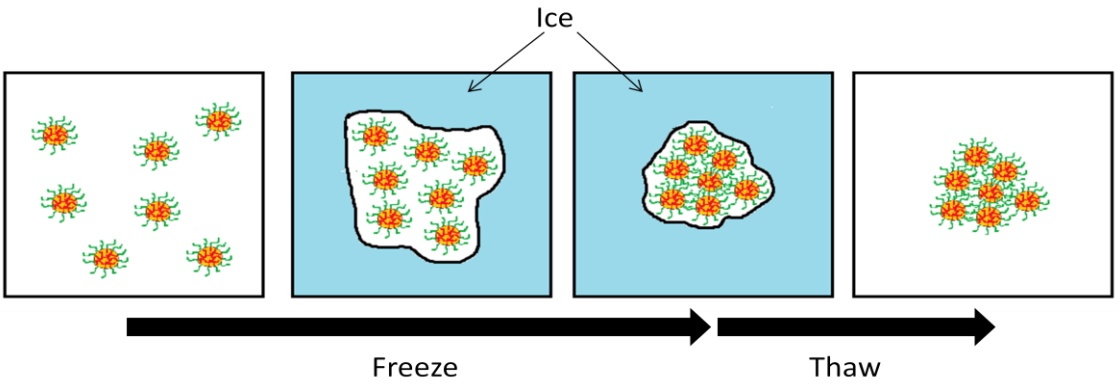

Figure 4.3: Phase separation of the nanoparticle suspension into ice and a cryo-concentrated solution. The particles are expelled into an area of higher and higher concentration. As a result the nanoparticles are driven together, which could cause them to aggregate.

even irreversible fusion of the nanoparticles. Additionally, the crystallization of ice may exert a mechanical stress on particles leading to their destabilization [61]. To understand the effect of freezing on particle size a simple freeze thaw study was carried out on the nanoparticles. The particles were first frozen in liquid nitrogen for 15 minutes and then

allowed to heat back up to room temperature. DLS was used to analyze nanoparticle size both before and after freezing.

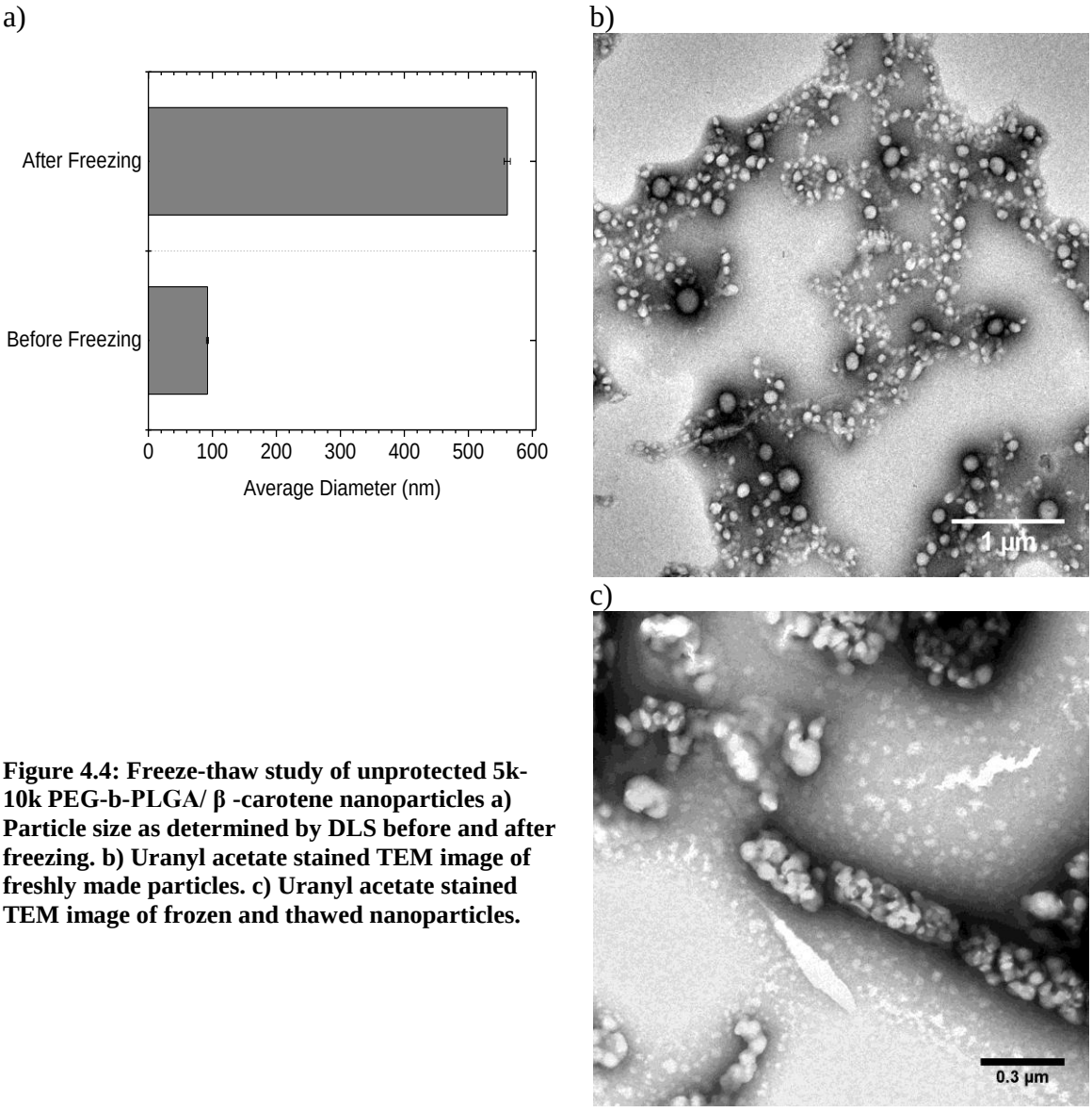

Figure 4.4: Freeze-thaw study of unprotected 5k-10k PEG-b-PLGA/ β -carotene nanoparticles a) Particle size as determined by DLS before and after freezing. b) Uranyl acetate stained TEM image of freshly made particles. c) Uranyl acetate stained TEM image of frozen and thawed nanoparticles.

Figure 4.4a shows a large increase in nanoparticle size as determined by DLS from approximately 100 nm to 550 nm. Figure 4.4b and c show TEM images of freshly made particles and particles after freezing and thawing, respectively. Before freezing and thawing, the particles appeared spread across the TEM grid, while after freezing they

appeared highly aggregated. It is clear that some sort of cryoprotectant must be used to stabilize the nanoparticles during the lyophilization process.

4.3.2. Addition of cryoprotectants

In order to protect nanoparticles from the various stresses of the lyophilization process, some sort of cryoprtotectant is normally added prior to freezing. In literature, the most popular cryprotectants for the freeze drying of nanoparticles are sugars such as trehalose, sucrose, glucose and mannitol [61]. These sugars are known to vitrify at a specific temperature known as T_g', or the glass transition temperature of a maximally cryo-concentrated solution [63]. As the water freezes, the nanoparticles and cryoprotectant are expelled into area of increasing concentration. As the liquid becomes more concentrated, its viscosity increases, inducing inhibition of further crystallization. The addition of a small amount of sugar will therefore increase in concentration during freezing until the temperature reaches T_g', at which point the sucrose solution will vitrify. Figures 4.5 and 4.6 show a phase diagram and cartoon of the freezing process in the presence of cryprotectants, respectively. DSC of a 20 wt% sucrose solution showed a T_g' of -33.3^{o}C, as shown in figure 4.7. The immobilization of the nanoparticles within a glassy cryoprotectant matrix can prevent their aggregation and protect the particles against the mechanical stress of ice crystals [61]. In general, the type of cryoprotectant must be selected and its concentration optimized to ensure a maximum stabilization of nanoparticles. For this reason, a freeze thaw study should be carried out before freeze drying to select the best cryoprotectant.

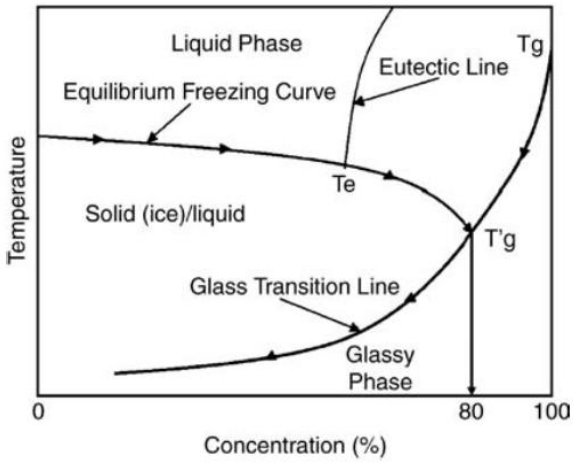

Figure 4.5: Phase diagram for a binary system of sucrose and water showing T_g' [60]

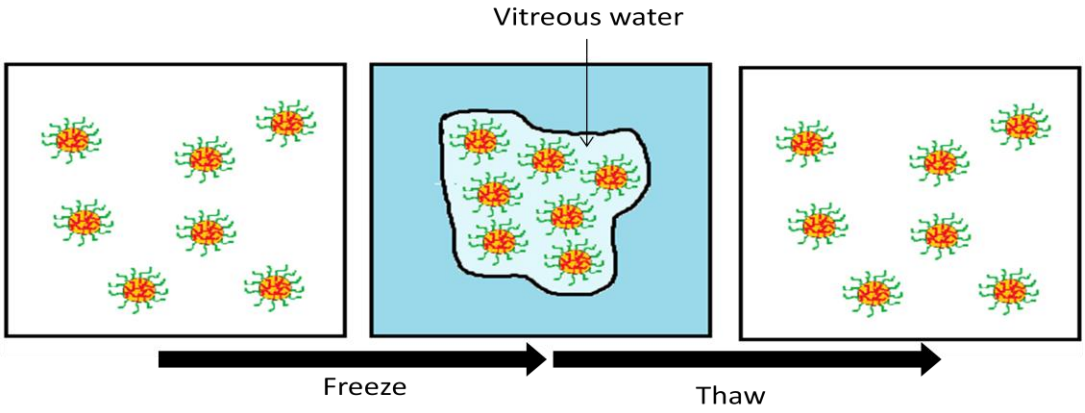

Figure 4.6: Phase separation of a nanoparticle suspension into a cryo-concentrated phase and ice in the presence of a cryoprotectant. The cryoprotectant is also expelled into areas of higher concentration. At a high enough concentration, the water will not freeze, but instead for a glassy matrix which can protect the nanoparticles from the mechanical stresses of ice crystals.

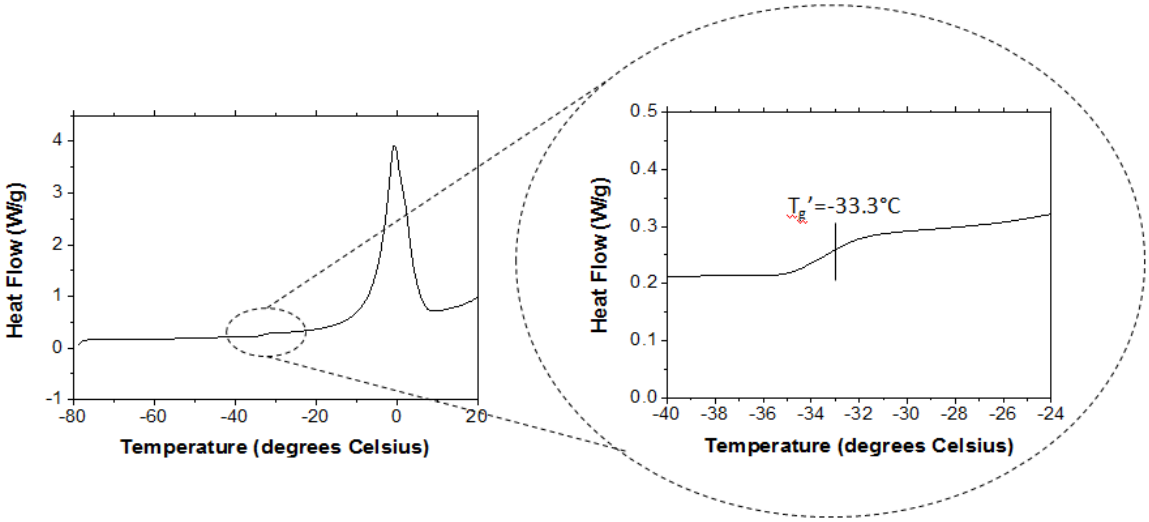

Figure 4.7: DSC curve for a 20 wt% sucrose in water solution. The curve shown is for heating of the solution from -80°C to 20°C. T_g' occurred at a temperature of -33.3°C.

Sucrose was chosen as a possible cryoprotectant for the 5k-10k PEG-PLGA/ β -carotene system. A freeze thaw study was performed using concentrations of sucrose varying from 0 mg to 60 mg of sucrose/mg of nanoparticle. After the particles were made, the sample was split, sucrose was dissolved at the appropriate concentration, and the sample was frozen in liquid nitrogen for 15 minutes. After freezing, the samples were allowed to thaw and then particle size was analyzed by DLS.

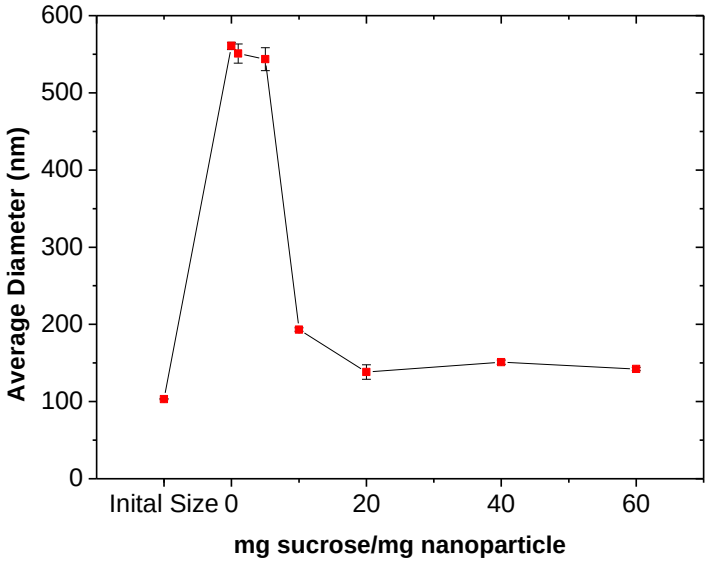

Figure 4.8: Freeze-thaw of 5k-10k PEG-b-PLGA/β-carotene nanoparticles using sucrose as a cryoprotectant. Approximately 10 mg of sucrose/ mg of nanoparticles was needed to achieve size recovery.

Sucrose played a clear role in preventing the aggregation of nanoparticles during the freezing process, as shown in figure 4.8. The addition of sucrose before freezing led to a much better size recovery after freezing. However, in order to get a good size recovery, a large amount of sucrose was needed. Such large amount of sucrose are troubling from a delivery point of view as large amounts of sucrose could lead to a high osmotic strength in the redispersed sample. Therefore, a cryoprotectant that needs a lower concentration to achieve a high level of protection during freezing would be ideal.

Pluronic F68, a block copolymer of poly(ethylene oxide)-poly(propylene oxide)-poly(ethylene oxide) (PEO-PPO-PEO) with a molecular weight of ~8400 was tested as a cryoprotectant. Few studies in the literature deal with the effect of surfactants, such as Pluronc F68, in the preservation of nanoparticle integrity after freeze drying as they are often already present in the original formulation [64]. Pluronic F68 was chosen as it has been used for the stabilization of nanoparticle dispersions [65] and as a cryoprotectant for both animal and plant culture systems [66]. Additionally, Pluronic F68 has been

described as safe for intravenous administration [67]. Therefore, a freeze thaw study similar to the one using sucrose was performed.

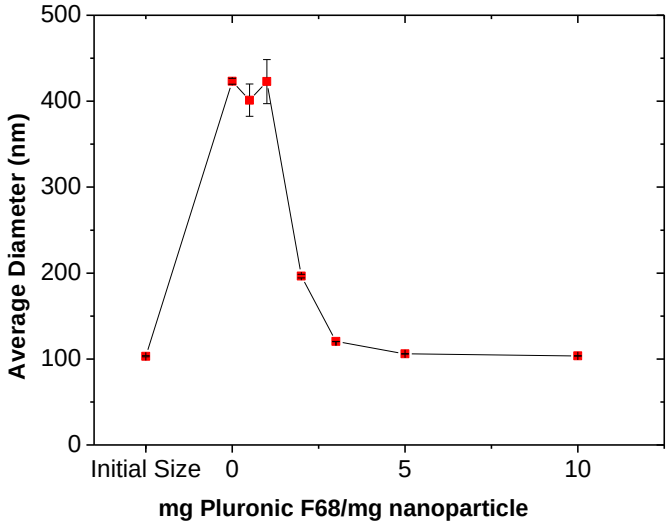

Figure 4.9: Freeze thaw study of 5k-10k PEG-b-PLGA using Pluronic F68 as a cryoprotectant. Size recovery was achieved using much lower amounts of Pluronic F68 (3mg/mg nanoparticles) than sucrose (10mg/mg nanoparticles).

Figure 4.9 shows a size recovery at much lower concentrations than when sucrose was used. The addition of 3 mg of Pluronic F68/mg of nanoparticle resulted in particles very close to their original size, whereas the use of sucrose resulted in nanoparticles 30-40 nm larger than their original size even at the highest concentrations of sucrose. Previous studies by Layre et al. [64] have shown that the use of surfactant was found to be the key for the production of freeze dried nanoparticles with high redipsersibility and low aggregation behavior. In addition, Layre found that much less surfactant was needed to prevent nanoparticle aggregation than sucrose, trehalose, and maltose. However, unlike the use of glucose, which showed a clear T_g' at -33.3°C, a DSC curve for a 20 wt% Pluronic F68 solution did not give a clear reason for its cryoprotective efficiency, as shown in figure 4.10. The DSC curve did show a possible T_g' at -67.9°C but also displayed transitions at -41.6° and -16.7°C.

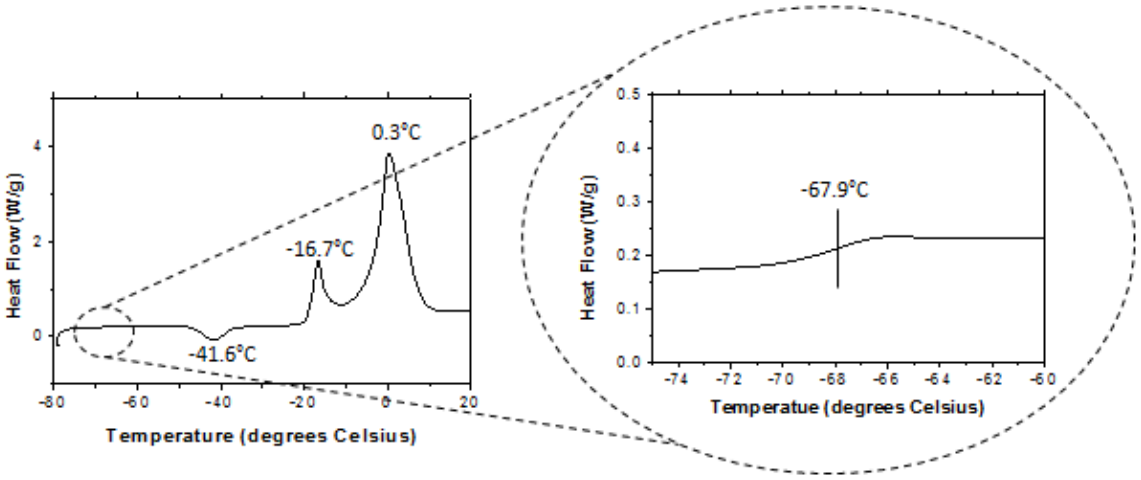

Figure 4.10: DSC curve of a 20 wt% Pluronic F68 solution. The solution was first cooled to -80°C. The curve shown is upon heating at 10°C/min.

4.3.3. Freeze drying

While freezing exerts mechanical stresses on the nanoparticle system that could cause them to aggregate and become unstable, the drying step also exerts stresses on the particle that could lead to their instability. The dehydration step involves the removal of ice and unfrozen water under vacuum. The primary driving step removes the ice from the sample by sublimation, while the secondary drying step involves the removal of water that did not separate out as ice during the freezing process [61]. It is important to remove the absorbed water from the sample because it is usually present in enough quantities to cause rapid decomposition of the product when it is stored at room temperatures. This is particularly important for biodegradable polymers such as PLGA, which can undergo hydrolysis, and drugs that react in the presence of water.

A good cryoprotectant not only protects the particles during the freezing process, but also during the dehydration step. A suggested stabilization mechanism of nanoparticles during the drying step is the water replacement hypothesis. The lyoprotective effect of cryoprotectants, such as sugars, during the drying process is due to

their ability to act as a "water substitute" through hydrogen bonding with polar groups at the surface of the nanoparticles [59]. The lyoprotectants preserve the native structures of the nanoparticles. In addition, the amorphous state of nanoparticles and lyoprotectant allows maximal hydrogen bonding between nanoparticles and stabilizer molecules. It is therefore important to choose a stabilizer that remains amorphous throughout the drying process, as crystallization results in a limited formation of hydrogen bonds and less effective preservation [62]. Special care also must be taken when freeze drying PEG coated nanoparticles. While PEG allows for prolonged circulation in vivo, the presence of PEG at the surface is a challenge during the freeze drying process. PEG is known to crystallize during this process, leading to dramatic nanoparticle aggregation [68].

The cryoprotective efficiency of Pluronic F68 and sucrose during the freeze drying process was studied due to their ability to protect the particles during the freezing process. Based on the freeze thaw studies, Pluronic F68 was added to the nanoparticle suspension at a concentration of 3 mg Pluronic F68/mg nanoparticle, while sucrose was added at 10 mg sucrose/mg nanoparticle. The samples were then frozen in liquid nitrogen and placed under vacuum. When the water had been removed from the samples, they were rehydrated and sonicated with a probe sonicator over a period of eight minutes. The particle size was analyzed both before freezing, after rehydration, and every two minutes during sonication. A similar procedure was carried out using unprotected nanoparticles.

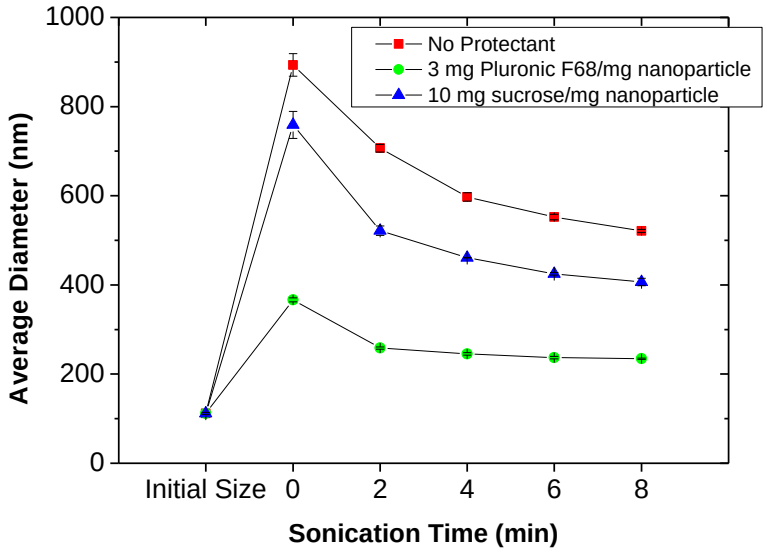

Figure 4.11: Redispersion of protected and unprotected freeze dried 5k-10k PEG-b-PLGA/ β-carotene nanoparticles. The particles containing 3 mg pluronic F68/mg nanoparticle redispersed the best, while those containing no protectant and the worst size recovery.

From figure 4.11, it is clear that the addition of a cryoprotectant is necessary in order to achieve effective particle recovery after freeze drying. While full particle size recovery was not achieved with the addition of Pluronic F68, it was much better than the unprotected particles and those containing sucrose. Much less energy was also required to redisperse the cryo-protected nanoparticles. The unprotected particles continued to decrease in size over the entire sonication period, while the Pluronic F68 protected nanoparticles were fully redispersed after two minutes and additional sonication lead to no change in particle size.

Ease of redispersion is an important aspect for freeze dried nanoparticles. Often times, aggregation is undone through the use of high energy redispersion. However, medical settings don't always have access to such methods and it is not always practical or convenient to use them. High energy redispersion could also either rupture the particles or cause the suspension to heat up past the particle melting point. Therefore, a low energy method for the redispersion of lyophilized nanoparticles close to the initial size is important. A clear difference was observed between particles freeze dried with

protectant and without protectant after rehydration, as shown in figure 4.12. Prior to sonication, the rehydrated sample containing 3 mg Pluronic/mg nanoparticle redispersed and appeared homogenous with no extra sonication, while the unprotected particles remained in large aggregates and did not easily redisperse.

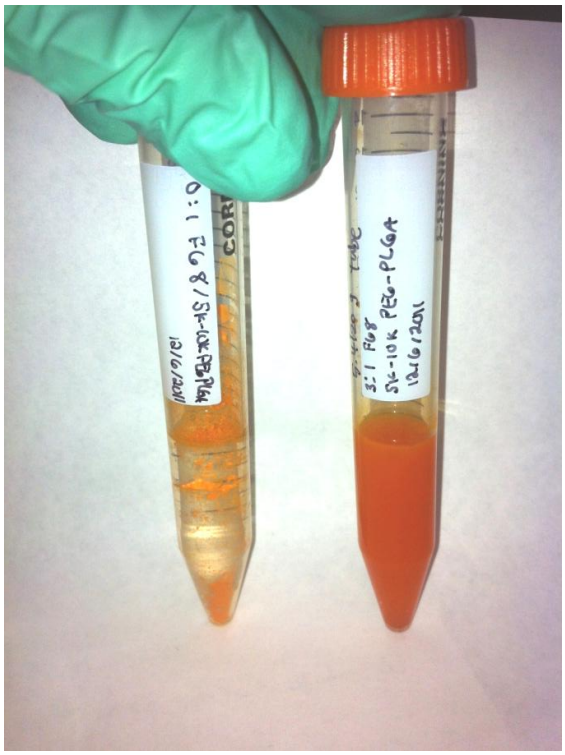

Figure 4.12: Rehydrated 5k-10k PEG-b-PLGA/ β -carotene nanoparticles before sonication. The sample on the left contains no protectant, while the sample on the right contains 3 mg pluronic/mg nanoparticle. The sample containing no protectant remained in large aggregates, while that containing pluronic F68 appeared much more homogenous.

4.3.4. Paclitaxel silicate prodrug loaded nanoparticles

Due to the effective use of Pluronic F68 at stabilizing 5k-10k PEG-PLGA/ β -carotene nanopaticles made by flash nanoprecipitation, the effect of the addition of Pluronic F68 to a paclitaxel prodrug nanoparticle was studied. Paclitaxel is a hydrophobic anticancer drug. Previous work using flash nanoprecipitation to encapsulate paclitaxel into a 5k-10k PEG-PLGA block copolymer showed that the particles were unstable and underwent rapid growth due to Ostwald ripening. However, the conjugation of the drug to a silicate ester to form a more hydrophobic prodrug enabled the formation

of stable nanoparticles [27, 42]. During administration, the paclitaxel silicate prodrug can undergo hydrolysis back to its active form in vivo [55]. In this case, a bis-triethylsilicate paclitaxel prodrug was used. It is important for the cryoprotectant to have a similar effect on the prodrug loaded nanoparticles as these particles will be used in actual applications. Similar to the β -carotene loaded particles, 3 mg of pluronic F68/mg of nanoparticle was added to the nanoparticle suspension before freezing.

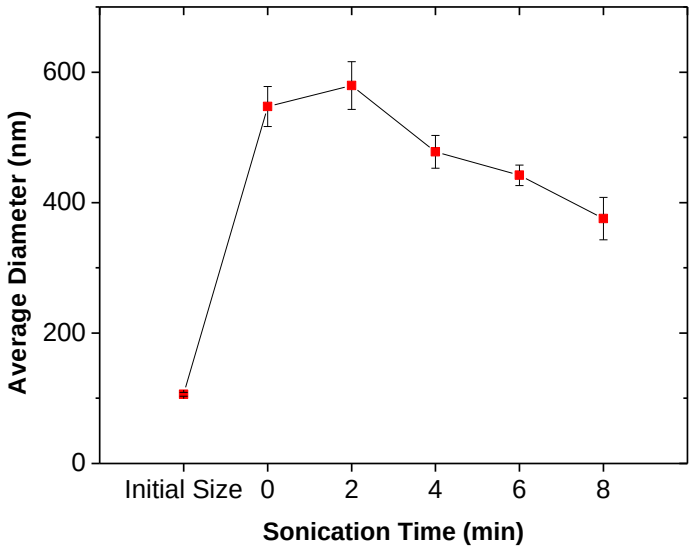

Figure 4.13: Redispersion of 5k-10k PEG-b-PLGA/ bis-triethylsilicate paclitaxel prodrug loaded nanoparticles freeze dried with 3mg Pluronic F68/mg nanoparticle. The particles did not have as good of a size recovery as the 5k-10k PEG-b-PLGA nanoparticles that were freeze dried with 3 mg pluronic F68/mg nanoparticle

The paclitaxel prodrug loaded nanoparticles did not redisperse nearly as well as the β-carotene loaded nanoparticles, as shown in figure 4.13. This was verified by cryo-TEM, as seen in figure 4.14. Before freeze drying, the particles appeared well dispersed and spherical. However, after freeze drying and redispersion both with and without a cryoprotectant the particles were largely aggregated and deformed.

a)

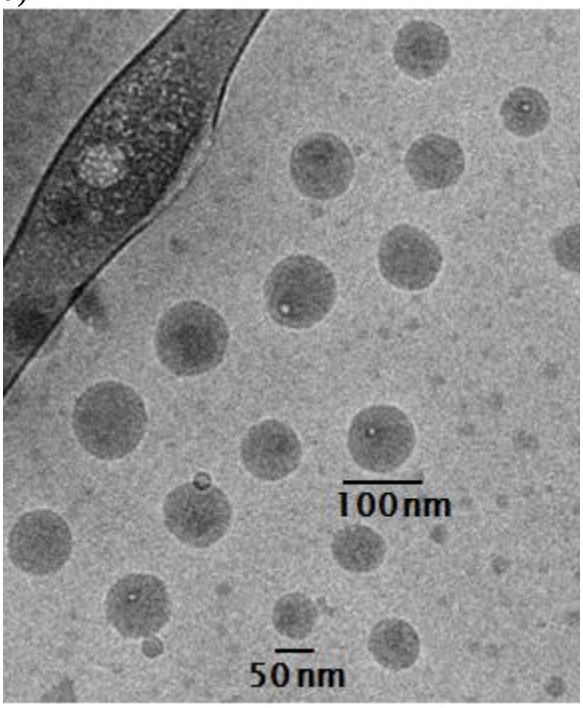

b)

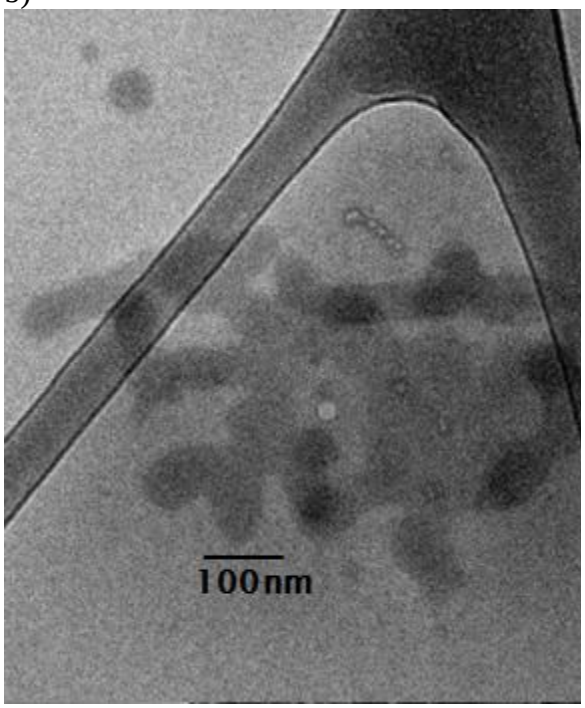

c)

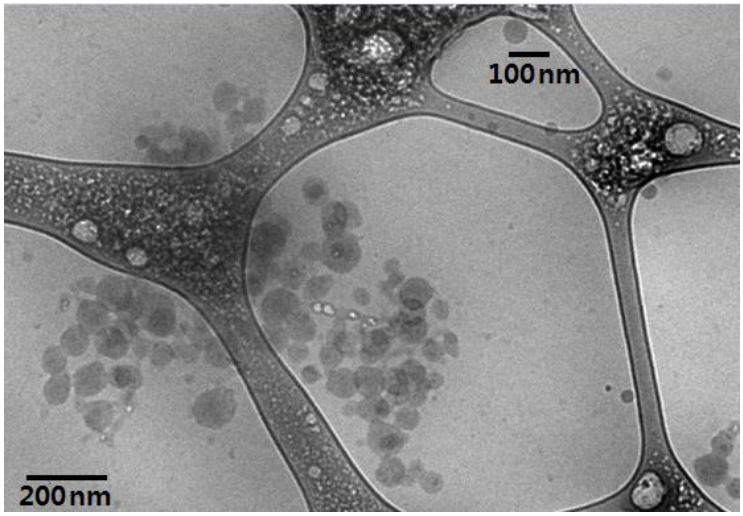

Figure 4.14: Cryo-TEM images of 5k-10k PEG-b-PLGA/ bis-triethylsilicate paclitaxel prodrug nanoparticles a) before Freeze drying b) after freeze drying with no protectant c) after freeze drying using 3mg pluronic F68/mg nanoparticle. Before freeze frying the particles appear to be well dispersed and spherical. After freeze drying, the particles were in large aggregates whether or not a cryoprotectant was used.

Even with the addition of Pluronic F68 before freezing, aggregation of the particles occurs. This shows that not only the polymer being used is important, but also the drug being loaded into the particle. In order for particles to be effectively delivered

via the EPR effect, particles need to be less than 200 nm. This shows the importance of finding the optimum formulation for the redispersion of different particles.

4.3.5. Effect of block copolymer

So far, the block copolymer being used to formulate the nanoparticles was a 5k-10k PEG-b-PLGA. This amphiphilic BCP was chosen due to its biocompatibility, biodegradability, and its ability to make stable nanoparticles in suspension. However, it is possible to make nanoparticles using different BCP's and also BCP's of varying molecular weight. In this case, particles made using 5k-5k PEG-b-PLA and 5k-10k PEG-b-PLA were compared to the 5k-10k PEG-b-PLGA nanoparticles. While previous studies showed that 5k-10k PEG-b-PLGA nanoparticles were the most stable in suspension, they are not necessarily the most stable and redispersible after freeze drying. After the nanoparticles were formulated, they were freeze dried with no cryoprotectant and 3 mg Pluronic F68/mg nanoparticles

a)

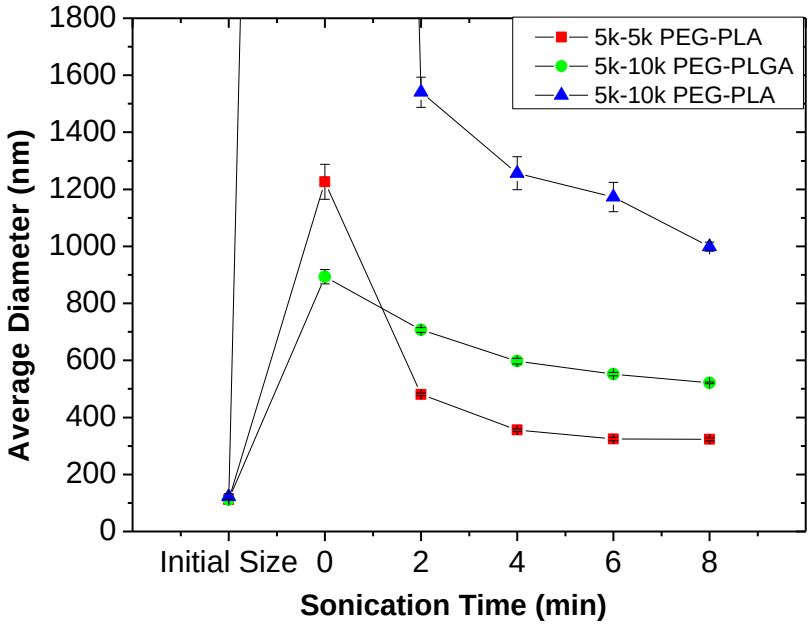

b)

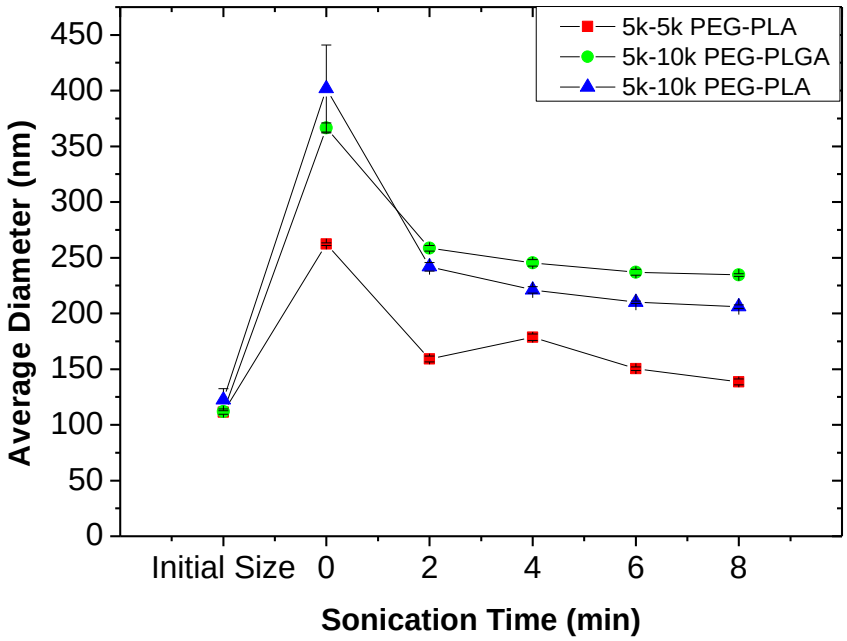

Figure 4.15: Redispersed nanoparticles made using 5k-5k PEG-b-PLGA, 5k-10k PEG-b-PLA, and 5k-10k PEG-b-PLGA. All particles were made using β-carotene as the model drug. The particles were freeze dried using a) no protectant and b) 3mg Pluronic F68/mg nanoparticle. In each of the cases, the 5k-5k PEG-b-PLA nanoparticles had the best size recovery.

In both case, the 5k-5k PEG-b-PLA showed the best final size recovery, as shown in figure 4.15. While the exact cause of the difference in redispersibility is not yet known, one can speculate that it is likely due to a larger surface coverage by the PEG on the outside of the nanoparticles. In nucleation and growth, the hydrophobic drug or drug model first nucleates. Following nucleation, the particle continues to grow until the amphiphilic block copolymer covers the surface, which will arrest the growth. In order for the hydrophobic block to cover the entire surface of the particle, a larger number of chains of the 5k-5k PEG-b-PLA block copolymer would be needed than for the 5k-10k block copolymer. This would lead to a larger PEG chain density on the outside of the particles. This higher chain density could then prevent the entanglement of PEG chains between particles during freeze drying, and therefore an easier redispersibility. This

could also explain the difference in the redispersion of the 5k-10k PEG-b-PLA and 5k-10k PEG-b-PLGA nanoparticles. Previous studies showed that 5k-10k PEG-b-PLA were not stable in a saline solution, likely due to the particles being partially electrostatically stabilized. When the salt was added, the particle surface charge was neutralized. The lack of steric stabilization was hypothesized as being due to the solubility parameters between the two blocks of the block copolymer. The PEG and PLA block have a higher affinity for one another than PEG and PLGA, likely causing some of the PEG to be trapped by the PLA and therefore less surface coverage by the PEG [27]. Less PEG on the surface would therefore result in a lower chain density on the particle surface and a decrease in redispersibility.

4.4. Future work

While progress has been made in the freeze drying procedure for PEG-b-PLGA nanoparticles made via FNP, the redispersed nanoparticles are still not ideal for injection. In addition, other important parameters, such as stability upon storage and drug phase, have not been analyzed. The following is a list of parameters that should be studied in order to better understand the freeze drying process and hopefully result in stable, easily redispersible nanoparticles.

4.4.1. Importance of storage

Long term stability is often required after freeze drying. From an application point of view, the particles should be formulated, freeze dried, and remain stable until they are resuspended for clinical use. The stability of the nanoparticles involves the chemical and physical stability of the particles. This includes the prevention of degradation reactions for both the polymer stabilizer and drug used to formulate the

nanoparticles. In order for nanoparticles made by FNP to be feasible in a clinical setting, their long term stability must be understood. Therefore, the long term stability of the particles should be studied.

The nanoparticle stability study should be carried out at several ambient conditions over a period of several months. The nanoparticles can be stored at room temperature, 25^{o}C, in order to determine particle stability for nanoparticles being stored under normal conditions. Every month, the size and drug loading would then be evaluated to detect instability of the nanoparticles. Additionally, particles should also be studied at lower temperatures. Previous studies have shown an increased particle stability after freeze drying when particles were stored at 4^{o}C vs. 25^{o}C [69].

4.4.2. Freezing and drying temperature

So far, only the concentration and type of cryoprotectant has been analyzed for the stabilization of freeze dried nanoparticles. However, as stated previously, additional process parameters such as freezing rate and temperature, colloidal concentration, and drying time and temperature can all affect the ease at which the dried powder can be resuspended back to its original size. These variables must therefore be further analyzed.

The effect of drying and freezing temperature are important criteria that were not analyzed during the freeze drying that took place in this study. Due to equipment limitations, all of the freeze dried samples were frozen in liquid nitrogen and then freeze dried in a room temperature container. The effectiveness of cryoprotectants during freeze drying comes from their ability to form an amorphous matrix around the particles. The cryoprotectants vitrify at a specific temperature known as T_g'. In order to design an optimum freeze drying process, critical properties of the optimized formulation must be

known. These include the glass transition temperature of the frozen sample (T_g') and the collapse temperature of the formulation, T_c. The collapse temperature is the maximum allowable temperature during primary drying. Above T_c, the freeze dried product loses macroscopic structure and collapses during freeze drying [70]. Collapse is the result of a glass transition in the dried region formed during primary drying. T_c can often be estimated as being several degrees above T_g'. The difference in T_g' and T_c is subtle and due to the difference in concentration in the dried region. Water is removed from the amorphous phase one the ice-vapor interface passes by the region of interest. Since water removal increases the viscosity, viscous flow and therefore collapse is arrested and the effective collapse temperature is increased [71].

In order to ensure total solidification of a sample, the nanoparticle suspension must be cooled below the T_g' of the formulation. This will ensure that particles are trapped in the vitreous cyro-concentrated solution as opposed to remaining in an aqueous environment. Therefore, freezing temperature is important during the freeze drying process. In addition, cooling rate has also been shown to have an effect on the redispersibility of freeze dried nanoparticles. In some cases, a fast cooling leads to more easily redispersible particles, while in other cases slow freezing improved freeze drying [62]. Since only liquid nitrogen was used to cool the particles, freezing took place at a relatively fast rate. Future work needs to study how the freezing rate and temperature could affect the redispersibility of freeze-dried nanoparticles.

The drying temperature has also been shown to have a large impact on the freeze drying process. This is due to the collapse temperature of the frozen product. A high residual water content and a long reconstitution time are common consequences of

collapse in a product. This is most likely due to the lack of porous structure in the final product [72]. In the current study, the temperature of the sample during freeze drying was not controlled. In order to optimize the freeze drying process, the drying temperature must be controlled so that it remains below the collapse temperature of the sample.

4.4.3. Other cryoprotectants

So far, only Pluronic F68 and sucrose have been studied to determine their affect on the freeze drying of 5k-10k PEG-b-PLGA nanoparticles made by FNP. However, the use of many other sugars and their effect on cryoprotective efficiency has been studied. Trehalose, for example, seems to be more preferred as a cryoprotectant for nanoparticles [61]. Compared to other sugars, it has an absence of internal hydrogen bonds which allows for more flexible formation of hydrogen bonds during freeze drying. Additionally, it has a very low chemical reactivity and a higher glass transition temperature than many other sugars. A higher glass transition temperature means that the samples can be frozen at a higher temperature, and since the collapse temperature is usually about 2^{o}C higher than T_g', the drying process can also take place at a higher temperature.

In addition to using cyroprotectants other than sucrose and Pluronic F68, a mixture of cryoprotectants should also be explored. Layre et al. [64] found a mixture of Poloxomer 188 and trehalose lead to the best redispersion of nanoparticles, even at low cryoprotectant concentrations. In their study, they found the poly(ethylene glycol)-b-poly(caprolactone) (PEG-b-PCL) nanoparticles could be redispersed without significant aggregation at a cryoprotectant to nanoparticle ratio of 0.5/1 (w/w). When only trehalose was used, some aggregation occurred even at a 10/1 ratio of cryoprotectant to

nanoparticle, while a 2/1 ratio of poloxamer 188 was needed to prevent aggregation. Therefore, the simultaneous addition of a sugar and a surfactant should be explored for the preservation of our PEG-b-PLGA nanoparticles.

4.4.4. Nanoparticle concentration

Nanoparticle concentration has a crucial effect on the success of freeze drying. In a previous study by De Jaeghere et al. [59], poly(ethylene glycol)-b-poly(ethylene oxide) nanoparticles were freeze dried with varying concentrations of lyoprotectant, which in this case was trehalose. They found that regardless of the amount of lyoprotectant, the concentration of the suspension prior to freeze drying played a key role. Higher nanoparticle concentrations lead to higher lyoprotective efficiency. Even at the high weight rate ratios of trehalose to nanoparticle (10:1), the suspension could not be redispersed when the suspension was at a 0.2 wt% concentration. At a 0.8 wt% nanoparticle concentration, however, total preservation of the nanoparticle size was achieved using a 2:1 trehalose to nanoparticle ratio.

The freeze drying of nanoparticles made by FNP in this study has all taken place at concentrations of 0.1 wt%. While several attempts were made to change the concentration by altering the formulation, they proved to be unsuccessful (as shown in chapter 2). One possibility is using a MicroKros® hollow fiber modules from Spectrum Labs [73]. These modules are designed for the cross flow filtration of small volumes. In order to concentrate the sample, two retentate syringes connected to luer inlet and outlet ports pass the sample back and forth through the membrane lumen while a third syringe collects the filtrate on a side port, as shown in figure 4.16.

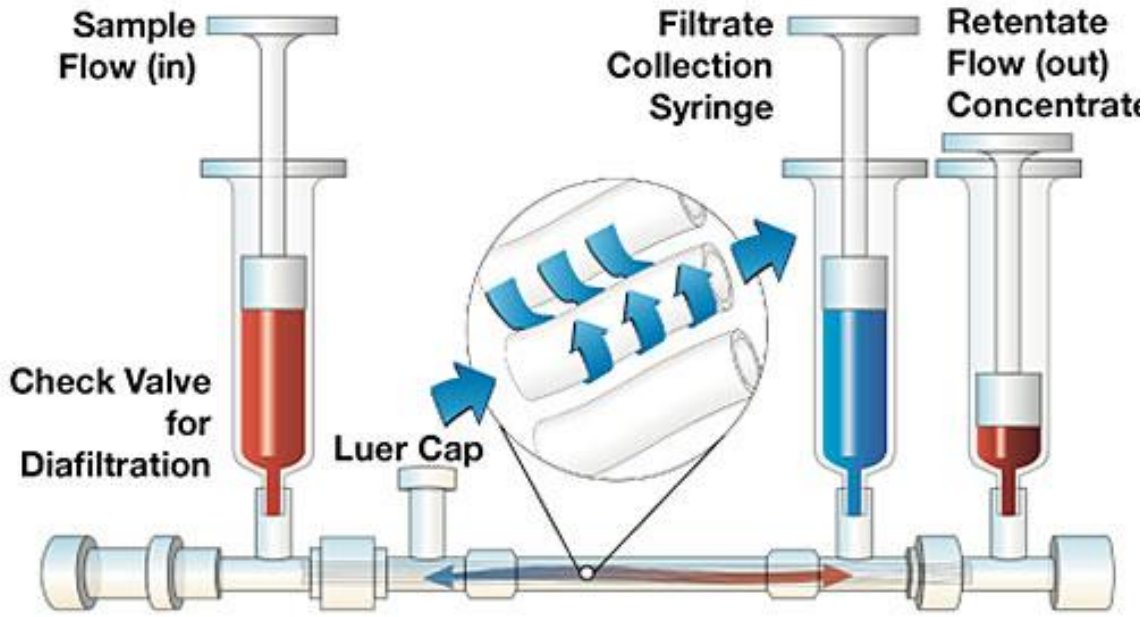

Figure 4.16: Schematic of the hollow fiber diafiltration membrane [73]

Initial results using 5k-b-10k PEG-PLGA nanoparticles showed that the nanoparticle suspensions could be concentrated to concentrations from 0.1 to as high as 2.5 wt%. Additionally, the mass of nanoparticles in both the filtrate and retentate stream was determined by freeze drying both samples. This resulted in all of the nanoparticles remaining in the retentate stream, while no particles passed through the filter into the filtrate collection syringe. Therefore, using these hollow fiber filtration membranes is a possible way to concentrate the particles for a more effective freeze drying process.

4.4.5. Phase of the drug

The phase of the drug in the nanoparticles strongly influences its bioavailability. Amorphous compounds offer significantly higher dissolution rates for hydrophobic compounds, leading to higher bioavailability. It is therefore important to know the morphology of the drug in the nanoparticle to determine its effect on bioavailability and achieve reproducible pharmacokinetic profiles. In previous work, X-ray diffraction

(XRD) was used to determine the crystalline nature of the nanoparticles [27]. Particles were made with 5k-10k PEG-b-PLGA and β-carotene by flash nanoprecipitation using the vortex mixer. Wet powder samples were prepared via centrifugal filtration and XRD was performed within 4 hours. The β-carotene was highly amorphous as the XRD traces did not show any crystalline peak. The amorphous state of the nanoparticles was likely due to the THF diffusing rapidly into the water phase and the large β-carotene molecules did not have enough time to align and pack tightly. However, this was the case for β-carotene nanoparticles that were not freeze dried. As stated previously, it is well known that the outer PEG corona of the nanoparticles crystallizes during the freezing process. In order to determine the morphology of the drug after freeze drying, XRD should be performed. Oh et al. [65] used XRD to analyze PTX-loaded Pluronic F-68 nanoparticles. In this case, nanoparticles were formed by a temperature induced phase transition. They found that the PTX-loaded nanoparticles showed a significant decrease in the crystalline peak of PTX, suggesting that the PTX was most likely in an amorphous state. However, these particles were made differently than our PEG-b-PLGA particles and freeze drying was not employed. XRD should therefore be used to characterize our freeze dried powder. One must be careful, however, as problems can arise in characterization of the crystal phases due to the reduced crystal length scales (i.e. very small crystals).

4.5. Conclusions

Flash nanoprecipitiation is an effective way to formulate hydrophobic drugs in a polymeric nanoparticle drug delivery system. FNP is able to generate particles in the ~100 nm size range, which is ideal for the delivery of many hydrophobic drugs, particularly cancer drugs due to their ability to localize in tumors via the EPR effect.

However, their translation to clinical use is a major obstacle. Freeze drying is one method by which the particles can be transformed into a solid of sufficient stability for storage.

In this study, the effect of freeze drying on nanoparticle stability and redispersibility was analyzed. Freeze-thaw studies clearly indicated that the particles would not be redispersible without the use of a sufficient cryoprotectant. Sucrose and Pluronic F68 were both used to determine what affect they would have during the lyophilization process. Pluronic F68 appeared to be the more effective cryoprotectant for the redispersion of the β-carotene loaded nanoparticles.

While the addition of Pluronic F68 resulted in much better redispersion of the 5k-10k PEG-b-PLGA/β-carotene nanoparticles, there are many factors that could result in much better nanoparticle redispersion after freeze drying. Initial studies showed that while a 5k-10k PEG-b-PLGA may result in the most stable nanoparticles in suspension, other block copolymers may result in a much better redispersibility. Additionally, sample freezing rate, freeze drying temperature, nanoparticle concentration, and the choice of cryoprotectant could all have a large impact on the freeze drying process. The ability to freeze dry nanoparticles and preserve their size and structure continues to be a major issue for the PEG-b-PLGA nanoparticles made by FNP. The goal of FNP is to make nanoparticles that can passively target tumors via the EPR effect. While the original particle sizes do fit into the range needed for passive tumor targeting, aggregation caused by freeze drying makes them less than ideal. The use of different formulations and parameters in freeze drying should therefore continue to be studied in the hope of

reaching an optimum procedure for the freeze drying and redispersion of drug loaded nanoparticles made via FNP.

References

[1] C. Lipinski, Poor aqueous solubility - An industry wide problem in drug discovery, Am. Pharm. Rev. 5 (2002) 82-85.

[2] Bristol-Myers Squib Company, TAXOL (R) (paclitaxel) INJECTION, (2007). (http://packageinserts.bms.com/pi/pi_taxol.pdf)

[3] A.J. Tije, W.J. Loos, A. Sparreboom, Pharmacological effects of formulation vehicles: implications for cancer chemotherapy, Clin. Pharmacokinet. 42 (2003) 665-658.

[4] R.B. Weiss, R.C. Donehower, P.H. Wiernik, Hypersensitivity reactions from Taxol, J. Clin. Oncol. 8 (1990) 1263-1268.

[5] Abraxis Bioscience, ABRAXANE (R) (paclitaxel-bound particles for injectable suspension), (2006). (www.abraxane.com)

[6] U.S. Food and Drug Administration, ABRAXANE for injectable suspension (paclitaxel protein-bound particles for injectable suspension) (albumin-bound), (2005).(http://dailymed.nlm.nih.gov/dailymed/archives/fdaDrugInfo.cfm?archiveid=13954)

[7] M. Goldberg, R. Langer, X. Jia, Nanostructured materials for applications in drug delivery and tissue engineering., J. Biomat. Sci., Polym. Ed. 18 (2007) 241-68.

[8] L. Brannon-Peppas, J.O. Blanchette, Nanoparticle and targeted systems for cancer therapy., Adv. Drug Delivery Rev. 56 (2004) 1649-59.

[9] Y. Matsumura, H. Maeda, A new concept for macromolecular therapeutics in cancer chemotherapy: Mechanism of tumor tropic accumulation of proteins and antitumor agent SMANCS, Cancer Res. 46 (1986) 6387-6392.

[10] J. Folkman, Angiogenesis in cancer, vascular, rheumatoid and other disease, Nat. Med. 1 (1995) 27-31.

[11] H. Maeda, J. Wu, T. Sawa, Y. Matsumura, K. Hori, Tumor vascular permeability and the EPR effect in macromolecular therapeutics: a review., J. Controlled Release. 65 (2000) 271-84.

[12] S. Skinner, Microvascular architecture of experimental colon tumors on the rat, Cancer Res. 50 (1990) 2411-2417.

[13] A. Gabizon, Long-circulating liposomes for drug delivery in cancer therapy: a review of biodistribution studies in tumor-bearing animals, Adv. Drug Delivery Rev. 24 (1997) 337-344.

[14] G. Kong, R.D. Braun, M.W. Dewirst, Hyperthermia enables tumor specific nanoparticle delivery: effect of particle size, Cancer Res. 60 (2000).

[15] S. Bisht, A. Maitra, Dextran-doxorubicin/chitosan nanoparticles for solid tumor therapy, WIREs Nanomed. Nanobiotechnol. 1 (2009) 415-425.

[16] S. Kim, Liposomes as carriers of cancer chemotherapy- Current status and future prospects, Drugs. 46 (1993) 618-638.

[17] D.E. Discher, A. Eisenberg, Polymer vesicles., Science (New York, N.Y.). 297 (2002) 967-73.

[18] G. Kwon, Diblock copolymer nanoparticles for drug delivery, Crit. Rev. Ther. Drug Carrier Syst. 15 (1998) 481-512.

[19] C. Allen, Nano-engineering block copolymer aggregates for drug delivery, Colloids Surf., B. 16 (1999) 3-27.

[20] F. Ahmed, R.I. Pakunlu, A. Brannan, F. Bates, T. Minko, D.E. Discher, Biodegradable polymersomes loaded with both paclitaxel and doxorubicin permeate and shrink tumors, inducing apoptosis in proportion to accumulated drug., J. Controlled Release. 116 (2006) 150-8.

[21] P.P. Ghoroghchian, J.J. Lin, A.K. Brannan, P.R. Frail, F.S. Bates, M.J. Therien, et al., Quantitative membrane loading of polymer vesicles, Soft Matter. 2 (2006) 973.

[22] K. Kataoka, T. Matsumoto, M. Yokoyama, T. Okano, Doxorubicin-loaded poly(ethylene glycol)-polu(beta-benzyl-l-apspartate) copolymer micelles: their pharmaceutical characteristics and biological significance, J. Controlled Release. 64 (2000) 143-153.

[23] B.K. Johnson, R.K. Prud'homme, Chemical processing and micromixing in confined impinging jets, AIChE Journal. 49 (2003) 2264-2282.

[24] B.K. Johnson, R.K. Prud'homme, Flash NanoPrecipitation of Organic Actives and Block Copolymers using a Confined Impinging Jets Mixer, Aust. J. Chem. 56 (2003) 1021.

[25] M.C. Brick, H.J. Palmer, T.H. Whitesides, Formation of Colloidal Dispersions of Organic Materials in Aqueous Media by Solvent Shifting †, Langmuir. 19 (2003) 6367-6380.

[26] J. Aubry, F. Ganachaud, J-P. Cohen Addad, B. Cabane, Nanoprecipitation of polymethylmethacrylate by solvent shifting: 1. Boundaries., Langmuir. 25 (2009) 1970-9.

[27] Z. Zhu, Polymer stabilized nanosuspensions formed via flash nanoprecipitation: nanoparticle formation, formulation, and stability [PhD thesis], University of Minnesota, 2010.

[28] Y. Liu, Z. Tong, R.K. Prud, Stabilized polymeric nanoparticles for controlled and efficient release of bifenthrin, Spectrum. 812 (2008) 808-812.

[29] J. Baldyga, R. Pohorecki, Turbulent micromixing in chemical reactors- a review, Chem. Eng. J. 58 (1995) 183-195.

[30] M. Chaubal, Polylactides/glycolides-excipients for injectable drug delivery and beyond, Drug Delivery Technology. 2 (2002) 34–36.

[31] V.O. Sheftel, Indirect Food Additives and Polymers: Migration and Toxicology, CRC Press, 2000.

[32] Y. Li, Y. Pei, X. Zhang, Z. Gu, Z. Zhou, W. Yuan, et al., PEGylated PLGA nanoparticles as protein carriers: synthesis, preparation and biodistribution in rats., J. Controlled Release. 71 (2001) 203-11.

[33] F. Alexis, E. Pridgen, L.K. Molnar, O.C. Farokhzad, Factors affecting the clearance and biodistribution of polymeric nanoparticles., Mol. Pharmaceutics. 5 (2008) 505-15.

[34] Y. Hu, J. Xie, Y.W. Tong, C-H. Wang, Effect of PEG conformation and particle size on the cellular uptake efficiency of nanoparticles with the HepG2 cells., J. Controlled Release. 118 (2007) 7-17.

[35] S.M. D'Addio, C. Kafka, M. Akbulut, P. Beattie, W. Saad, M. Herrera, et al., Novel Method for Concentrating and Drying Polymeric Nanoparticles : Hydrogen Bonding Coacervate Precipitation, Mol. Pharmaceutics. 7 (2010) 557-564.

[36] H. Lee, H. Fonge, B. Hoang, R.M. Reilly, C. Allen, The effects of particle size and molecular targeting on the intratumoral and subcellular distribution of polymeric nanoparticles, Mol. Pharmaceutics. 7 (2010) 1195-1208.

[37] C. Fang, B. Shi, Y.-Y. Pei, M.-H. Hong, J. Wu, H.-Z. Chen, In vivo tumor targeting of tumor necrosis factor-alpha-loaded stealth nanoparticles: effect of MePEG molecular weight and particle size., Eur. J. Pharm. Sci. 27 (2006) 27-36.

[38] ACD/Labs, www.acdlabs.com

[39] H. Qian, A.R. Wohl, J.T. Crow, C.W. Macosko, T.R. Hoye, A Strategy for Control of "Random" Copolymerization of Lactide and Glycolide: Application to Synthesis of PEG-b-PLGA Block Polymers Having Narrow Dispersity., Macromolecules. 44 (2011) 7132-7140.

[40] B.G.G. Lohmeijer, R.C. Pratt, F. Leibfarth, J.W. Logan, D. A. Long, A.P. Dove, et al., Guanidine and Amidine Organocatalysts for Ring-Opening Polymerization of Cyclic Esters, Macromolecules. 39 (2006) 8574-8583.

[41] B.K. Johnson, R.K. Prud'homme, Process and apparatuses for preparing nanoparticle compositions with amphiphilic copolymers and their use, U.S. Patent US20040091546, 2004.

[42] J. Han, Block Copolymer Protected Paclitaxel-based Nanoparticle Formulation in Drug Delivery System, Dossier-University of Minnesota. (2010).

[43] Dynamic Light Scattering : An Introduction in 30 Minutes, Malvern Instruments, (http://www.malvern.com/common/downloads/campaign/MRK656-01.pdf)

[44] D.E. Koppel, Analysis of macromolecular polydispersity in intensity correlation spectroscopy: the method of cumulants, J. Chem. Phys. 57 (1972) 4814.

[45] J. Jakes, Regularized positive exponential sum (REPES) program - a way of inverting laplace transform data obtained by dynamic light scattering, Collect. Czech. Chem. Commun. 60 (1995) 1781-1797.

[46] J.C. Thomas, The determination of log normal particle size distributions by dynamic light scattering, J. Colloid Interface Sci. 117 (1987) 187–192.

[47] A.J. Mahajan, D.J. Kirwan, Nucleation and growth kinetics of biochemicals measured at high supersaturations, J. Cryst. Growth. 144 (1994) 281-290.

[48] H. Shen, S. Hong, R.K. Prud'homme, Y. Liu, Self-assembling process of flash nanoprecipitation in a multi-inlet vortex mixer to produce drug-loaded polymeric nanoparticles, J. Nanopart. Res. 13 (2011) 4109-4120.

[49] J.C. Cheng, R.O. Fox, Kinetic modeling of nanoprecipitation using CFD coupled with a population balance, Ind. Eng. Chem. Res. 49 (2010) 10651-10662.

[50] J.C. Cheng, R.D. Vigil, R.O. Fox, A competitive aggregation model for flash nanoprecipitation., J. Colloid Interface Sci. 351 (2010) 330-42.

[51] M.E. Gindy, A.Z. Panagiotopoulos, R.K. Prud'homme, Composite block copolymer stabilized nanoparticles: simultaneous encapsulation of organic actives and inorganic nanostructures., Langmuir. 24 (2008) 83-90.

[52] R. Karnik, F. Gu, P. Basto, C. Cannizzaro, L. Dean, W. Kyei-Manu, et al., Microfluidic platform for controlled synthesis of polymeric nanoparticles., Nano Lett. 8 (2008) 2906-12.

[53] B. Testa, Prodrug research: futile or fertile?, Biochem. Pharmacol. 68 (2004) 2097-106.

[54] V.J. Stella, K.W. Nti-Addae, Prodrug strategies to overcome poor water solubility., Adv. Drug Delivery Rev. 59 (2007) 677-94.

[55] C.W. Macosko, T.R. Hoye, J. Panyam, Beyond Taxol (R): Nanoparticle Delivery of a Paclitaxel Silicate Prodrug, Minnesota Future Grant Proposal. (2009).

[56] R.W. Smith, The Staining of Polymers, Microsc. Microanal. 8 (2002) 190-191.

[57] Y. Matsumura, H. Maeda, A new concept for macromolecular therapeutics in cancer chemotherapy: mechanism of tumoritropic accumulation of proteins and the antitumor agent smancs., Cancer Research. 46 (1986) 6387-92.

[58] M. Chacón, J. Molpeceres, L. Berges, M. Guzmán, M.R. Aberturas, Stability and freeze-drying of cyclosporine loaded poly(D,L lactide-glycolide) carriers., Eur. J. Pharm. Sci. 8 (1999) 99-107.

[59] F. De Jaeghere, E. Allémann, J. Feijen, T. Kissel, E. Doelker, R. Gurny, Freeze-drying and lyopreservation of diblock and triblock poly(lactic acid)-poly(ethylene oxide) (PLA-PEO) copolymer nanoparticles., Pharm. Dev. Technol. 5 (2000) 473-483.

[60] F. Franks, Freeze-drying of bioproducts: putting principles into practice., Eur. J. Pharm. Biopharm. 45 (1998) 221-9.

[61] W. Abdelwahed, G. Degobert, S. Stainmesse, H. Fessi, Freeze-drying of nanoparticles: formulation, process and storage considerations., Adv. Drug Delivery Rev. 58 (2006) 1688-713.

[62] W. Abdelwahed, G. Degobert, H. Fessi, Investigation of nanocapsules stabilization by amorphous excipients during freeze-drying and storage., Eur. J. Pharm. Biopharm. 63 (2006) 87-94.

[63] L.L. Chang, D. Shepherd, J. Sun, D. Ouellette, K.L. Grant, X.C. Tang, et al., Mechanism of protein stabilization by sugars during freeze-drying and storage: native structure preservation, specific interaction, and/or immobilization in a glassy matrix?, J. Pharm. Sci. 94 (2005) 1427-44.

[64] A.M. Layre, P. Couvreur, J. Richard, D. Requier, N. Eddine Ghermani, R. Gref, Freeze-drying of composite core-shell nanoparticles., Drug Devel. Ind. Pharm. 32 (2006) 839-46.

[65] K.S. Oh, J.Y. Song, S.H. Cho, B.S. Lee, S.Y. Kim, K. Kim, et al., Paclitaxel-loaded Pluronic nanoparticles formed by a temperature-induced phase transition for cancer therapy., J. Controlled Release. 148 (2010) 344-50.

[66] P. Anthony, N.B. Jelodar, K.C. Lowe, J.B. Power, M.R. Davey, Pluronic F-68 Increases the Post-thaw Growth of Cryopreserved Plant Cells, Plant Cell. 514 (1996) 508-514.

[67] A. Floyd, Top ten considerations in the development of parenteral emulsions., Pharm. Sci. Technol. To. 4 (1999) 134-143.

[68] F. De Jaeghere, E. Allémann, J. Feijen, T. Kissel, E. Doelker, R. Gurny, Freeze-drying and lyopreservation of diblock and triblock poly(lactic acid)-poly(ethylene oxide) (PLA-PEO) copolymer nanoparticles., Pharm. Dev. Technol. 5 (2000) 473-83.

[69] A. Gursoy, L. Eroglu, M. Ta, H. Fessi, F. Puisieux, J.-philippe Devissaguet, Evaluation of indomethacin nanocapsules for their physical stability and inhibitory activity on inflammation and platelet aggregation, Int. J. Pharm. 52 (1989) 101-108.

[70] M.J. Pikal, R. Putman, The secondary drying stage of freeze drying : drying kinetics as a function of temperature and chamber pressure *, Int. J. Pharm. 60 (1990) 203-217.

[71] M.J. Pikal, S. Shah, The collapse temperature in freeze drying : Dependence on measurement methodology and rate of water removal from the glassy phase, Int. J. Pharm. 62 (1990) 165-186.

[72] Y.N. Konan, R. Gurny, E. Allémann, Preparation and characterization of sterile and freeze-dried sub-200 nm nanoparticles., Int. J. Pharm. 233 (2002) 239-52.

[73] Spectrum Labs, www.spectrumlabs.com.

Appendix A.1: Particle Size Characterization

Dynamic Light Scattering (DLS) was the main tool used for the characterization of nanoparticle size. Different analysis techniques allow for the analysis of multimodal particle sizes. The purpose of this appendix is to analyze the ability of DLS to determine the particle size for a highly polydisperse sample.

Dynamic Light Scattering

DLS is a technique for the measuring the size of particles, typically in the sub micron region. DLS measures the time dependent fluctuations in the scattering intensity to determine the translational diffusion coefficient (D_T) and subsequently the hydrodynamic radius of the particles via the Stokes Einstein Equation.

$$R_H = \frac{k_b T}{6\pi\eta_s D_T}$$

Eq. A.1

R_H is the hydrodynamic radius, k_b is Boltzmann's constant, T is temperature, η_s is the solvent viscosity, and D_T is the translational diffusion coefficient.

In scattering experiments, the intensity of the scattered light depends on time since the scattering centers are in constant random motion due to their kinetic energy. The variation in the scattering intensity with time will then contain information on the random motion of the particles and can be used to measure the diffusion coefficient of the particles. This random motion of the particles is known as Brownian motion. Brownian motion is the random movement of the particles due to their bombardment by the solvent molecules that surround them. In DLS, the speed at which the particles are diffusing due to Brownian motion is determined by the rate at which the intensity of scattered light fluctuates when detected using a suitable optical arrangement. The rate at which these

fluctuations occur will depend on the size of the particles. Small particles will move more quickly than large particles due to them being "kicked" further by the solvent molecules. This results in a faster decaying fluctuation.

In a typical DLS experiment, a detector measures the time-dependence of the intensity of the light over a period of time. The intensity I(s) fluctuates around an average value because of the random motion of the scatterers. In order to be able to use the fluctuation of the intensity around the average value, the fluctuations need to be represented in a convenient manner. Although $I_s(t)$ looks much like noise, it actually has a typical time constant which corresponds to the correlation time over which the signal loses memory. However, it is not convenient to deal with detailed records of the fluctuation of a measured quantity as a function of time. Instead, the details of the fluctuations is reduced to a time autocorrelation function, C(s,t) [1].

$$C(s,t) = \lim_{T\to\infty} \frac{1}{T} \int_0^T I(s,t')I(s,t'+t)dt'$$

Eq. A.2

The autocorrelation function involve taking the intensity at some time t' and multiplying it by the intensity some time t later, and then adding the results up over some long time period T. By dividing by T, the length of time of the experiment is then taken out of the equation. The autocorrelation function has its highest value at t=0. As $t\to\infty$, I(t') and $I_s(t'+t)$ become uncorrelated and C(t) becomes independent of t. By dividing the autocorrelation function by its asymptotic value, the overall averaged intensity autocorrelation function can be written as eq. A.3 [2].

$$\frac{C(s,t)}{(\overline{I(s)})^2} = g_2(s,t) = 1 + \beta|g_1(s,t)|^2$$

Eq. A.3

This equation is known as the siegert relation, in which β is an instrumental constant approximately equal to unity, and s is defined as $s \equiv |\vec{s}| = (4\pi n/\lambda)\sin(\theta/2)$ ($\vec{s}$ is a scattering vector), and t is the decay time. A digital correlator in the DLS instrument calculates the autocorrelation function automatically. The particles size can then be obtained from the correlation function using various algorithms. These include cumulants, CONTIN, and REPES.

In the case of monodisperse, spherical particles, $g_1(s,t)$ can be defined by a single exponential.

$$g_1(s,t) = A\exp(-s^2 D_T t)$$

Eq. A.5

A is a coefficient. Using this relation, the diffusion coefficient, D_T, can be found. The Stokes Einstein equation can then be used to determine the hydrodynamic radius, and therefore diameter, of the particle.

For a bimodal species, $g_1(s,t)$ can be described by a sum of two exponential.

$$g_1(s,t) = A_1\exp\left(-s^2 D_{T,1} t\right) + A_2\exp\left(-s^2 D_{T,2} t\right)$$

Eq. A.6

A_1 and A_2 are coefficients and $D_{T,1}$ and $D_{T,2}$ are the diffusion coefficients for the two different size particles in the sample. However, when the sample becomes more polydisperse $g_1(s,t)$ is not a simple exponential. It is in these cases that an algorithm such as cumulants, CONTIN, or REPES must be used [3]. The method of cumulants is the simplest method for determining the size of a polydisperse nanoparticle sample.

Cumulants fits a single exponential to the correlation function to obtain the means size and an estimate of the width of the distribution. The validity of the cumulant fit rests on the assumption that the distribution is a Gaussian or normal curve in log space [4]. CONTIN fits a multiple exponential to the correlation function to obtain a distribution of particle sizes [5]. REPES, which stands for regularized positive exponential sum, yields a series of discrete particle diameter to represent the particle size distribution [6].

Originally, particle size was being reported as the mass average size of the particles as determined by the REPES algorithm. The intensity (d_I), mass (d_m) and number (d_n) average sizes as determined by DLS are shown in equations A.7, A.8 and A.9, respectively.

$$d_I = \frac{\sum n_i d_i^6}{\sum n_i d_i^5} \qquad d_m = \frac{\sum n_i d_i^4}{\sum n_i d_i^3} \qquad d_n = \frac{\sum n_i d_i}{\sum n_i}$$

Eq. A.7 Eq. A.8 Eq. A.9

n_i is the number of particles and d_i is the particle diameter

DLS measurements were performed on a commercial Brookhaven ZetaPALS instrument located in the lab of Dr. Michael Tsapatsis. Zhu made a comparison of particle size determined using scanning electron microscopy (SEM) images and DLS. He found that the number average size of the particles determined by DLS was much smaller than that determined by SEM, and that the mass average size of the particles determined using the DLS and the REPES software was much more comparable to that determined by SEM. Since DLS provided results much more quickly than SEM and image analysis, the mass average size as determined by DLS using the REPES algorithm was reported [7]. However, based on earlier results, the validity of this technique needed to be reanalyzed.

Standard latex samples of monodisperse polystyrene spheres were ordered from Ted Pella, Inc. Spheres of size 30 nm, 90 nm and 173 nm were purchased and had coefficients of variation of ≤18%, ≤5%, and ≤3% respectively [8]. Particle size was determined by a combination of dynamic light scattering and optical microscopy. In order to verify DLS as a way to determine the size of our nanoparticle suspensions, the 90 nm standard was used. The particles were delivered at a 0.1wt% solution, which is the same concentration at which we make our nanoparticles. Therefore, the first test was to determine if the Brookhaven DLS instrument being used could accurately measure the size of the 90 nm standard particle at this concentration. An undiluted sample of the 90 nm standard was prepared, analyzed by DLS, and the data was fit using the REPES algorithm and particle size was reported as the mass average diameter. As can be seen in figure 5, the DLS grossly underestimated the size of the particles. The 90 nm standard sample prepared at 0.1 wt% gave an average diameter of 29 nm when measured by DLS and REPES. However, after dilution of the particles, the DLS and REPES algorithm accurately reported the particle size with an average diameter of 88 nm. Similar results were observed using the 173 nm standard, with mass average diameters of 114 nm and 173 nm being reported for the undiluted and dilute samples, respectively.

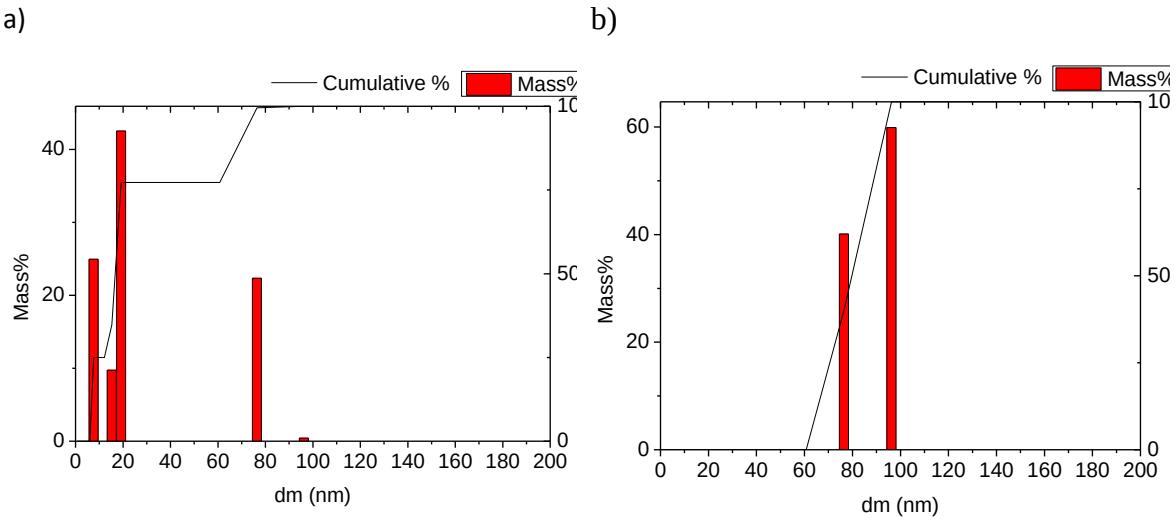

Figure A.1: a) 90 nm standard analyzed by DLS and REPES at 0.1 wt% concentration b) 90nm standard analyzed by DLS and REPES at 0.001 wt%. The mass average sizes for the 0.1 wt% and 0.001 wt % solutions as determined by DLS and REPES were 29 and 88 nm, respectively.

The underestimate in particle size was most likely due to a phenomenon called the multiple scattering artefact. In a diluted solution, a photon is scattered once before being detected by the photo-detector. In a concentrated solution, however, several scattering events can occur since the particles are closer to each other. This interferes with the correlation calculations and usually leads to an underestimate in the hydrodynamic radius [9]. Therefore, the method by which particle size was determined had to be altered.

The advantage of using algorithms such as REPES and CONTIN is their ability to pick up the particle sizes for a polydisperse sample. In order to verify the accuracy at which DLS can determine the particle size for a multimodal sample, mixtures of the polystyrene latex samples were mixed together and then analyzed by DLS. According to the manufacturer, the latex particles contain 6.74×10^{13}, 2.5×10^{12}, and 3.7×10^{11} spheres per cubic centimeter for the 30nm, 90nm, and 173nm samples, respectively [8]. By mixing these samples in various ratios, the average particle size can be predicted. Using equations A.7-A.9, the intensity, weight, and number average sizes can be

determined and compared to the values determined by the method of cumulants, CONTIN, and REPES. As previously stated, the method of cumulants fits a single exponential to the data to get an average particle size as well as a measure of the distribution. Since the method of cumulants assumes a lognormal distribution, the result can be transformed to yield both an mass average and number average particle size [4]. The Brookhaven DLS instrument gives a measure of the intensity, mass and number average size as determined by cumulants, as well as sizes determined by CONTIN. The raw data can be taken and further analyzed using the REPES algorithm. In this case, GENDIST, as software program developed by Jakes was used to generate the intensity distribution using the REPES algorithm. Table A.1 expected average particle sizes and the particle sizes as determined by cumulants, CONTIN and REPES for the polystyrene latex standard mixtures.

a)

	Calculated	**Cumulants**	**CONTIN**	**REPES**
Mixture	d_i (nm)	d_i (nm)	d_i (nm)	d_i (nm)
30nm +90nm	84	90.7	86.3	89
90nm+173nm	156	163.1	179.3	194
30nm+173 nm	169	175.8	178.1	175
30nm+90nm+173nm	153.2	160.4	164.1	164

b)

	Calculated	**Cumulants**	**CONTIN**	**REPES**
Mixture	d_m (nm)	d_m (nm)	d_m (nm)	d_m (nm)
30nm +90nm	60	74.4	86.3	74
90nm+173nm	132.5	137.4	159.2	141
30nm+173 nm	103.3	172.1	203.8	143
30nm+90nm+173nm	98	145.3	138.5	142

c)

	Calculated	Cumulants	CONTIN
Mixture	d_n (nm)	d_n (nm)	d_n (nm)
30nm +90nm	32.1	59.4	86.3
90nm+173nm	100.7	113.1	136.4
30nm+173 nm	30.8	169.6	168.8
30nm+90nm+173nm	32.9	130.5	51.4

Table A.1: a) Intensity b) mass and c) number average sizes of mixtures of polystyrene latex particles as determined by dynamic light scattering.

From the results, it is clear that the intensity average diameter is the most accurate for the mixtures of the polystyrene latex standards. Dynamic light scattering is based on the intensity of scattered light. In calculating the mass and number average sizes, assumptions are made about the distribution and errors may be compounded as the data is further analyzed. In each case, the calculated particle size was smaller than that determined by DLS. This is likely due to the intensity of scattered light being proportional to the radius of the particles to the sixth power. The raw data is weighted more heavily to the larger particles, which could cause the discrepancies in going from intensity to mass to number average particle diameter. As a result, the average particle size should be reported as the intensity average particle size as determined by the method of cumulants.

References

[1] P.C. Hiemenz, T.P. Lodge, Polymer Chemistry, Second, Boca Raton, Fl, CRC Press, 2007.

[2] P.C. Hiemenz, R. Rajagopalan, Principles of Colloid and Surface Chemistry, Third Edit, Boca Raton, Fl, CRC Press, 1997.

[3] Dynamic Light Scattering : An Introduction in 30 Minutes, Malvern Instruments, (http://www.malvern.com/common/downloads/campaign/MRK656-01.pdf)

[4] J.C. Thomas, The determination of log normal particle size distributions by dynamic light scattering, J. Colloid Interface Sci. 117 (1987) 187–192.

[5] D.E. Koppel, Analysis of macromolecular polydispersity in intensity correlation spectroscopy: the method of cumulants, J. Chem. Phys. 57 (1972) 4814.

[6] J. Jakes, Regularized positive exponential sum (REPES) program - a way of inverting laplace transform data obtained by dynamic light scattering, Collect. Czech. Chem. Commun. 60 (1995) 1781-1797.

[7] Z. Zhu, Polymer stabilized nanosuspensions formed via flash nanoprecipitation: nanoparticle formation, formulation, and stability, 2010.

[8] Ted Pella, Inc, www.tedpella.com

[9] M. Connah, Unconventional Dynamic Light Scattering, NanoS Guide, (2007) 6-9.